



ING. MECATRÓNICA

**Tesis previa a la obtención del título de
Ingeniero en Mecatrónica.**

AUTOR: Gustavo Daniel Cerecerez Jiménez

TUTOR: Ing. Guillermo Alfredo Mosquera Canchingre

Diseño e Implementación de un Prototipo de Brazo Robótico
para el Empacado Automatizado de Pequeños Chocolates con
Inteligencia Artificial.

Design and Implementation of a Robotic Arm Prototype for
Automated Packaging of Small Chocolates with Artificial
Intelligence.

CERTIFICACIÓN DE AUTORÍA

Yo, Gustavo Daniel Cerecerez Jiménez, declaro bajo juramento que el trabajo aquí descrito es de mi autoría; que no ha sido presentado anteriormente para ningún grado o calificación profesional y que se ha consultado la bibliografía detallada.

Cedo mis derechos de propiedad intelectual a la Universidad Internacional del Ecuador, para que sea publicado y divulgado en internet, según lo establecido en la Ley de Propiedad Intelectual, reglamento y leyes.

A handwritten signature in black ink, appearing to read 'Gustavo Daniel Cerecerez Jiménez', written over a horizontal line.

C.I.: 1720598174

APROBACIÓN DEL TUTOR

Yo Guillermo Alfredo Mosquera Canchingre, certifico que conozco al autor del presente trabajo de titulación denominado "Diseño e Implementación de un Prototipo de Brazo Robótico para el Empacado Automatizado de Pequeños Chocolates con Inteligencia Artificial", Gustavo Daniel Cerecerez Jiménez siendo el responsable exclusivo tanto de su originalidad y autenticidad, como de su contenido.



Guillermo Alfredo Mosquera Canchingre

DIRECTOR DEL TRABAJO DE TITULACIÓN

ACKNOWLEDGMENTS

I extend my deepest gratitude to my mother, whose unwavering support and belief in me have been the bedrock of my academic journey. Her relentless guidance, understanding, and sacrifices have been my constant source of inspiration and strength. Her steadfast presence and encouragement in every step of my educational pursuit have been invaluable. In the same breath, I remember my father, his memory and the values he instilled in me continue to guide my path. I am grateful for the foundation he laid in my life, and I hope that my achievements honor his legacy.

I would also like to express my profound appreciation to Cristina, my partner, for her extraordinary support and understanding throughout this journey. Her constant encouragement, patience, and emotional strength have been a pillar of support for me. Her ability to inspire and motivate, coupled with her steadfast belief in my abilities, has been crucial in navigating the challenges of academia and in the successful completion of this thesis.

I owe a debt of gratitude to my friends from school, whose insightful advice has not only enriched my ideas but also helped in shaping my ideals. To my college friends, who I've had the fortune to meet on this academic path, I extend my heartfelt thanks for the laughter, the shared experiences during our studies, and their unwavering support that kept me moving forward, even in challenging times. Our collaborative successes are a testament to our joint efforts and camaraderie.

I am immensely thankful to my professors for their invaluable guidance, expertise, and mentorship. Their dedication to imparting knowledge and wisdom has significantly contributed to my academic growth and the success of this research. Their enthusiasm, engagement, and sharing of invaluable knowledge and experiences have profoundly influenced my professional growth.

CONTENTS

1	Mechanical design	1
1.1	Approach of the prototype	1
1.2	Technical specifications	2
1.3	Gripper Design	3
1.4	Links Design	9
1.5	Denavit-Hartenberg	17
1.6	Jacobians Matrix	18
1.7	Task-Space	19
1.8	C-Space	19
1.9	Work-Space	20
2	Electronic design	21
2.1	Component selection	21
2.2	Micro-Controller	21
2.3	5v Relay module	21
2.4	Vacuum Pump	22
2.5	Motors and drivers	23
2.6	CNC-Shield	24
2.7	Camera	25
2.8	Power supply	25
2.9	Electronic block diagram	26
3	Programming	27
3.1	Arduino Program	27
3.2	Object Detection program	28
3.3	Graphical User Interface (GUI)	30
3.4	Dataset	32
3.5	Confusion Matrix	35
4	Tests & Results	37
5	Total Costs	42

6	Conclusions	43
A	Mechanical drawings	49
B	Electronic drawings	61

LIST OF FIGURES

1	3D CAD Assembly.	2
2	Three Finger gripper design.	4
3	Bell design on gripper.	5
4	Grip concept of vaccum gripper	6
5	Grip concept of UVG.	7
6	Vacuum grip using salt.	9
7	Initial Link 1 design.	14
8	Original design analysis.	15
9	Original design deformation.	15
10	Re-designed piece.	16
11	Deformation of the re-design.	16
12	Frames positions.	17
13	Task-space of the PRR robot.	19
14	C-space of the PRR robot.	20
15	Work-Space of the PRR robot.	20
16	Arduino Uno board.	21
17	5v Relay module.	22
18	12v DC Motor Mini Air Pump.	22
19	NEMA-17 motor.	23
20	A4988 driver.	24
21	CNC-Shield.	24
22	Vmax Full HD Webcam.	25
23	Electronic block diagram.	26
24	Flowchart Arduino program.	28
25	Flowchart Object detection program.	29
26	Graphical User Interface developed.	31
27	Flowchart User Interface program.	32
28	Images taken for training.	33

29	Classes created for detection.	33
30	Training Time.	34
31	Training Results charts.	35
32	Confusion matrix obtained.	36
33	Images tested.	37
34	Real time view testing.	38
35	Array 1.	41
36	Array 2.	41

LIST OF TABLES

1	Robotic Arm Prototype Specifications.	3
2	Results table of tests with different fine-grained materials in the UVG. .	8
3	Grain size and moisture absorption of different fine-grained materials. .	8
4	Comparison of Grippers	9
5	Characteristics table of PLA.	14
6	Denavit-Hartenberg Parameters.	18
7	Summary of Image Augmentation Techniques	34
8	Results under controlled Lighting Conditions	39
9	Results under Variable Light Conditions	40
10	End Effector Performance Test Results	42
11	Total Costs	43

Design and Implementation of a Robotic Arm Prototype for Automated Packaging of Small Chocolates with Artificial Intelligence.

1. Mechanical design

This section describes the design and implementation of a robotic arm prototype for automated packaging of small chocolates with artificial intelligence, including its technical specifications, the 3D model designed in CAD software along with its corresponding calculations and the series of alternatives made regarding its components, such as the gripper and the links of the robotic arm.

1.1. Approach of the prototype

The prototype of the robotic arm, depicted in Figure 1, features a two-link configuration seamlessly integrated with a bell-shaped gripper. The arm's structure is reinforced by three 8mm stainless steel rods, providing robust support for the entire assembly. These rods are strategically aligned with three custom-designed bases, which serve to anchor the NEMA motors and support the links.

Additionally, the system incorporates a lead screw mechanism, facilitating precise movement of the links along the Z-axis. This feature enables a maximum extension of up to 34cm, rendering the robotic arm highly versatile and adaptable to a variety of scenarios.

This design ensures both stability and flexibility in the arm's operation, making it suitable for diverse applications. Mechanical drawings of the prototype can be found in Appendix A.

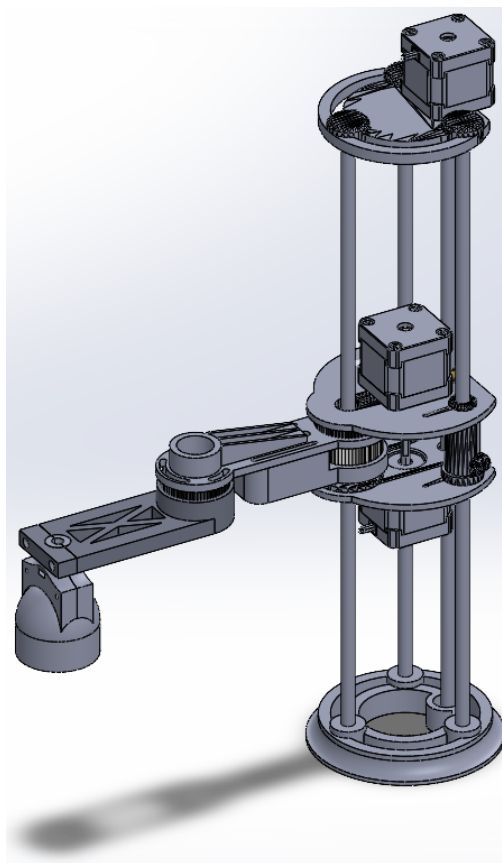


Figure 1. 3D CAD Assembly.

1.2. Technical specifications

Table 1 presents the key dimensional and structural specifications of the robotic arm prototype. This table is a concise summary of the prototype's physical characteristics, including its size, the length of its extendable parts, the range of movement in the Z-axis, the number of degrees of freedom (DOF), and the materials used in its construction.

The dimensions of the prototype are compact, measuring 10x10x45 cm, which indicates its suitability for operations in constrained spaces. The extension length of the links is 22 cm, providing a good range for reaching and manipulating objects. With a Z-axis displacement of 34 cm, the prototype demonstrates considerable versatility in vertical movement. The robotic arm possesses 3 degrees of freedom (DOF), enabling it to perform a variety of movements and tasks.

Finally, the table notes the primary materials used in the construction of the prototype: mostly PLA (Polylactic Acid) and Stainless Steel. These materials were chosen for their durability, strength, and suitability for the demands of the robotic arm's operations. This table is an essential reference for understanding the physical and structural attributes of the robotic arm prototype.

Specifications	Value
Robotic Arm Dimensions	10x10x45 cm
Extension length (Links)	22 cm
Z-Axis Displacement	34 cm
DOF	3
Materials	Mostly PLA & Stainless Steel
Work Area	Length: 36 cm ; Width: 20 cm

Table 1. Robotic Arm Prototype Specifications.

1.3. Gripper Design

The chocolates used in the project has a spherical and irregular shape. Its approximate diameter varies between 3 and 4 centimeters, which gives it a compact and rounded appearance. The average weight of each unit of Ferrero Rocher chocolate is approximately 4 grams. These physical characteristics of the chocolate were a determining factor when considering the design of the first gripper, which was initially designed with three fingers to achieve a precise and secure grip on each chocolate. The three-finger gripper was conceived as an initial solution for gripping Ferrero Rocher chocolates. Its main objective was to achieve an efficient and precise grip of the chocolates, allowing their manipulation and placement in the corresponding tray. Figure 2 shows the design concept of this gripper, its design consisted of three articulated fingers that adapted to the spherical and irregular shape of the chocolate. Each finger was intended to have the ability to partially envelop the chocolate, providing a firm yet gentle grip.

The approximate diameter of the Ferrero Rocher chocolate [1], between 3 and 4 centimeters, was a key factor considered in the design of the gripper fingers. The aim was to ensure that the fingers were flexible enough to adapt to the contour of the chocolate, without exerting excessive pressure that could damage it.

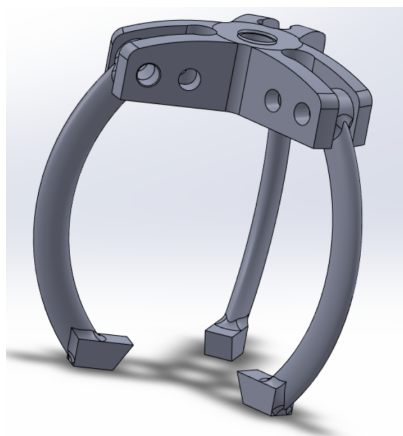


Figure 2. Three Finger gripper design.

However, the grip system presented various problems that hindered its efficiency and effectiveness. Firstly, there was the challenge of having enough space between the fingers of the claw to achieve a proper grip on the chocolate. Secondly, more space between the chocolate slots would be required to position the chocolate inside its corresponding slot in the plastic tray without interfering with the other chocolates due to the amount of space the claws needed. This meant that the gripper wouldn't be able to position the chocolates close enough together, this task required additional precision and careful handling during the handling process.

The determination of the grip force needed was also a significant challenge. A balance had to be found between the pressure exerted by the gripper's fingers to hold the chocolate without damaging it. Excessive force could deform or break the chocolate, while insufficient force did not ensure a secure and reliable grip.

Finally, the inclusion of force sensors to measure the pressure applied to the chocolate added complexity to the claw design. These sensors needed to be precisely integrated into the gripper's fingers to obtain accurate grip force measurements. The addition of sensors also required additional considerations in terms of wiring and calibration.

Given the situation, the use of the vacuum gripper [2] was considered to overcome the limitations and challenges associated with the three-finger gripper for handling Ferrero

Rocher chocolates. The objective was to implement a more efficient and reliable gripping system that would allow precise handling of the chocolates, avoiding damage and ensuring a smooth and efficient handling process, as well as reducing the necessary space and simplifying the design.

The vacuum grip system consisted of using the vacuum principle [3], to achieve a safe and stable grip of the chocolate. The clamp would use a bell with a line of silicone or other material that would conform to the chocolate as can be seen in the blue highlighted area in figure 3, creating a tight seal around it.

By generating a vacuum in the space between the bell and the chocolate, a gripping force would be achieved that would hold the chocolate in place without the need to apply excessive pressure. The goal was to achieve a gripping system that was more efficient in terms of time and design compared to the three-fingered claw.

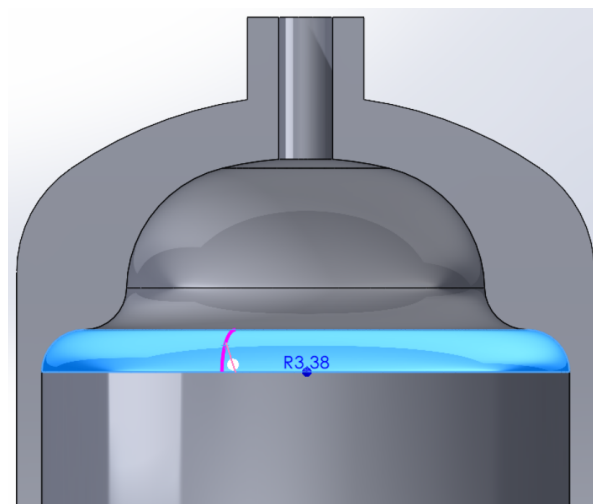


Figure 3. Bell design on gripper.

This system would allow faster handling and by not applying direct mechanical force to the chocolate, the risk of damaging it during the gripping process would be minimized as can be seen in figure 4.

During the implementation process of the vacuum gripper, several limitations and prob-

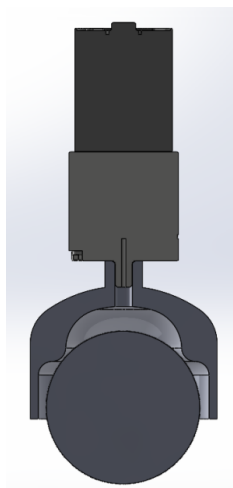


Figure 4. Grip concept of vacuum gripper

lems were faced that made it difficult for it to function optimally. One of the main limitations was in creating an isolated space between the gripper bell and the chocolate. Despite using silicone pads or other materials, air leaks were observed that did not allow the necessary vacuum to be generated for an effective grip. These leaks compromised the holding capacity of the chocolate and decreased the efficiency of the system.

In addition, to try to solve this problem, it was necessary to apply pressure on the bell of the gripper to make it adapt to the chocolate. However, this additional pressure caused damage to the chocolate, which was unacceptable due to the need to preserve the integrity of the product. These damages affected the presentation of the chocolate and compromised its quality.

These limitations were especially problematic considering the spherical and irregular nature of Ferrero Rocher chocolates. Its shape and characteristics made it even more difficult to grip accurately and safely with a conventional vacuum gripper.

The UVG (Universal Vacuum Gripper) [4] was discovered as an improved method to the second gripper design, being highly effective in gripping delicate objects, as seen on Figure 5. An adaptation and optimization process was carried out specifically for Ferrero Rocher chocolates. The system consists of three main components: a 3D-

printed bell, a balloon, and a fine-grained material.



Figure 5. Grip concept of UVG.

The custom-designed bell allows Ferrero Rocher chocolates to fit perfectly inside, ensuring a precise fit. On the other hand, the balloon plays a crucial role in the gripping process. When filled with fine-grained material, it acts as a container that holds the bonding material in place and prevents it from spreading.

The gripping process begins by drawing air out of the balloon with a mini air pump, causing the fine-grained material to compact around the product. This compression creates an intimate contact between the grains and the surface of the chocolates, generating a firm, secure and precise grip avoiding any unwanted movement.

Additionally, the balloon acts as a physical barrier between the salt and the chocolates, providing an additional layer of protection. This minimizes direct contact between the salt and the chocolates, significantly reducing the risk of damage to their surface by restricting the air pump discharge to fine grained material only.

By employing this method, it ensures that the appearance and quality of the Ferrero Rocher chocolates remain intact throughout the gripping process. To optimize the Universal Vacuum Gripper (UVG), a series of tests were conducted with various fine-grained materials, as detailed in Table 2. The objective was to identify the fine-grained material that exhibited superior performance, particularly in terms of compression and adaptability, ultimately leading to the most effective and efficient handling of the choco-

lates.

Table 2. Results table of tests with different fine-grained materials in the UVG.

Fine-Grained Material	Compression	Adaptability
Coffee	Efficient	Challenging
Sugar	Not viable	Not viable
Coffee + Sugar	Limited	Challenging
Salt	Efficient	Excellent

Firstly, coffee was considered, but it presented limitations in terms of its ability to recover its original shape after compression. In addition, it showed high moisture absorption, which affected its malleability and overall performance as a bonding material.

To address these challenges, a mixture of coffee and sugar was tested, considering the properties of both materials. However, this combination resulted in separation problems and failed to optimally fit the shape of the chocolates.

After extensive testing, it was decided to use salt as a fine-grained material in the UVG. This choice was based on its favorable characteristics, such as its ability to retain a stable shape after compression and its greater malleability compared to previous tests.

The salt demonstrated excellent conformability to the shape of the Ferrero Rocher chocolates, allowing precise gripping and rapid shape recovery when air pressure was released. Results of this test are shown in Table 3.

Table 3. Grain size and moisture absorption of different fine-grained materials.

Fine-Grained Material	Grain Size	Moisture Absorption
Coffee	Fine	High
Sugar	Coarse	Moderate-low
Coffee + Sugar	Varies	Varies
Salt	Medium	Low

When comparing the test results, it is clear that the salt outperformed the other materials tested. Its efficient compressibility, exceptional conformability and low moisture absorption make it the optimal material for UVG in the context of gripping Ferrero Rocher chocolate, as shown in Figure 6. This choice guarantees a safe and effective grip,

without compromising the integrity of the chocolates.



Figure 6. Vacuum grip using salt.

Table 4 summarizes the comparison of the different types of grippers that were considered throughout the project. In this case 5 is the maximum value reachable and 1 is the minimal. Depending on the category a higher value can be beneficial or unfavorable depending on the case.

Table 4. Comparison of Grippers

Category	3-Finger G.	Vacuum Gr.	UVG
Object adaptation	4	5	5
Construction Difficulty	4	2	3
Durability	4	5	5
Cost	3	2	2
Control difficulty	3	1	1
Maintenance	3	4	3
Power Requirements	3	3	3

1.4. Links Design

In the design of the robotic arm, special attention was given to the construction of its two primary links. These links are integral components of the arm's structure, each featuring meticulously designed gears that are integral to their function. The gears are not mere add-ons but are central to the arm's operational mechanics. They interact seamlessly with a series of toothed belts connected to the motors, forming a crucial

part of the movement transmission system.

These gears and belts are designed to work in harmony, ensuring smooth and precise movements of the robotic arm. This synergy is vital for the accurate and efficient execution of tasks, particularly in the delicate process of handling chocolates.

The combination of gears and toothed belts not only enhances the precision of movements but also contributes to the overall robustness and reliability of the robotic system. This thoughtful integration of components underscores the sophistication and effectiveness of the robotic arm's mechanical design.

For parts that are not subject to significant loads or stress, PLA was used instead of more rigid materials. PLA offers good rigidity for the current intended application and its printing is more accessible in terms of cost and availability [5]. However, it is important to highlight that the pieces were carefully designed to ensure their resistance and functionality.

TPU (thermoplastic polyurethane) [6] was chosen to manufacture the toothed belts. This choice is due to the fact that toothed belts with specific measurements were needed and they weren't available on the market. Printing this type of belts in TPU, resulted in a more precise and efficient assembly of the robot, due to the fact that they were customizable depending on the needs.

Calculations for toothed belt sizing factored in rotation speed, shaft diameter, and power transmission requirements. Considerations included the coefficient of friction, belt tension, and belt lifespan to maximize performance [7].

The following calculations ensured the selection of optimal gear sizes and ratios, motor power specifications, and gear profiles, facilitating smooth operation. For the gears it is required to make a series of calculations, which are indicated below.

1. Gear Module:

The gear module can be calculated with equation (1).

$$M = Ed/N + 2 \quad (1)$$

Where:

- M = Module of Gear.
- Ed = External Diameter.
- N = Number of teeth.

In this case a external diameter of 40mm and a number of teeth of 62 was selected. Replacing the values in the formula, a value of 0.625 was obtained for the module.

2. Primitive Diameter:

The primitive diameter of the gear can be calculated with equation (2).

$$Pd = M * N \quad (2)$$

Where:

- Pd = Primitive Diameter.
- M = Module of Gear.
- N = Number of teeth.

Replacing M for 0.625 and N with 62, a value of 38.75mm was obtained for the primitive diameter.

3. Internal Diameter:

The internal diameter of the gear can be calculated with equation (3).

$$Id = Pd - (2 * M) \quad (3)$$

Where:

- Id = Internal Diameter.
- Pd = Primitive Diameter.
- M = Module of Gear.

Replacing Pd with 38.75mm and M with 0.625 a value of 37.5mm was obtained for the internal diameter.

4. Circular Pitch:

The circular pitch of the gear can be calculated with equation (4).

$$P = \pi * M \quad (4)$$

Where:

- P = Circular Pitch.
- M = Module of Gear.

Replacing M with 0.625, a value of 1.96mm was obtained.

5. Space between teeth:

The space between the teeth of the gear can be calculated with equation (5).

$$St = P/2 \quad (5)$$

Where:

- St = Space between the teeth
- P = Circular Pitch.

Replacing P with 1.96mm, a value of 0.98mm was obtained for the space between the teeth of the gear.

6. Toothed Belts:

Two toothed belts of 160mm & 82 teeth and one toothed belt of 320mm & 164 teeth were used, giving a total of three belts. To define the number of teeth needed the following formula was used.(6).

$$N = D/P + 2. \quad (6)$$

Where:

- N=number of teeth
- D=measurement of the circumference of the belt
- P=Space Between teeth

These calculations were instrumental in ensuring the structural integrity and proper functioning of the gears and toothed belts in the robotic system. In addition, they allowed making informed decisions regarding the selection of materials and dimensions to achieve an efficient and reliable design.

Upon the initial assembly and activation of the robotic arm, complete with its gripper mechanism, a critical issue emerged in one of the arm's links. This particular link, distinctively marked in blue in Figure 7, forms a part of the complete robotic arm assembly as initially designed. The problem identified with link 1 was a direct consequence of the combined weight of link 2 and the gripper. This undue burden led to a noticeable bending in link 1, which introduced a degree of instability to the entire structure of the robotic arm.

This instability was not merely a minor inconvenience but posed a significant risk to the integrity of the system. The bending of link 1 indicated an impending mechanical failure, a scenario where continued operation could result in the link breaking. This would not only halt the operations of the arm but also potentially damage other components.

Such a breakage would be a setback to the project, necessitating redesign and repair. Hence, addressing this structural weakness was crucial for ensuring the reliability and durability of the robotic arm in its operational environment.

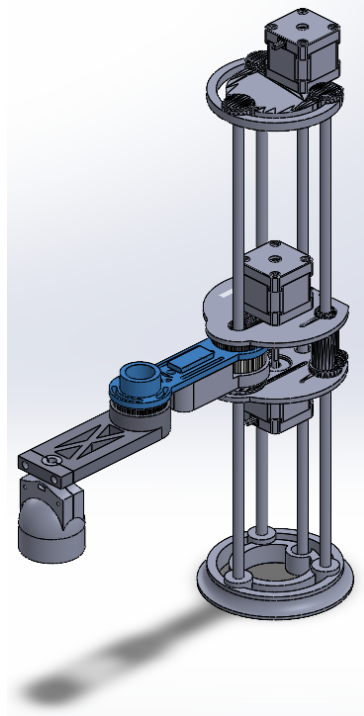


Figure 7. Initial Link 1 design.

The deformation analysis of the original part led to the decision of redesigning it to address the issue and improve its structural performance. The characteristics of the PLA material were considered during the analysis (Table 5) to better understand its properties.

Table 5. Characteristics table of PLA.

Property	Value	Unit
Elastic Module	2000000000	N/m ²
Poisson's ratio	0.394	N/D
Shear modulus	318900000	N/m ²
Mass density	1200	Kg/m ³
Tensile strength limit	50000000	N/m ²
Compression limit	40000000	N/m ²
Elastic limit	50000000	N/m ²
Coefficient of thermal expansion		/K
Thermal conductivity	0.2256	W/(m*K)

The initial design of the robotic arm was subjected to a comprehensive review to accurately determine the locations of both fixed and load-bearing surfaces, as depicted in

Figure 8. This step was crucial to understanding the mechanical stresses and potential points of failure within the structure. To quantitatively assess the stress distribution and deformation characteristics of the original design, finite element analysis (FEA) [8] simulations were carried out.

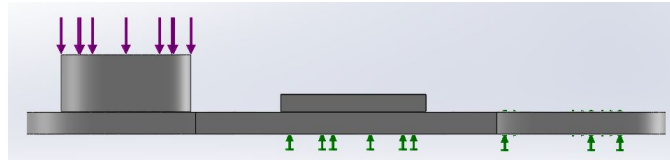


Figure 8. Original design analysis.

These simulations were performed using the SolidWorks software [9], a tool renowned for its precision and reliability in engineering design analysis. The primary focus was on link 1, where the initial problem of bending and potential breakage was observed. The results of the FEA provided a detailed visual representation of the deformation experienced by link 1 under operational loads, as clearly illustrated in Figure 9.

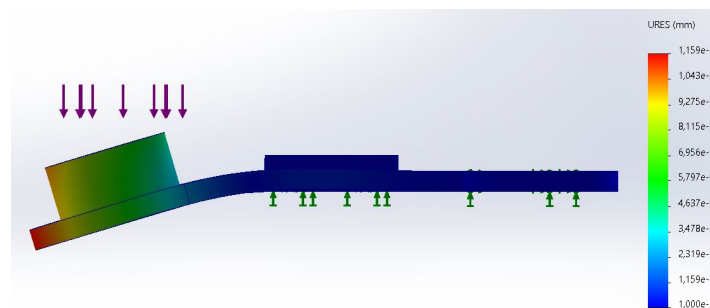


Figure 9. Original design deformation.

This analytical approach was instrumental in identifying the specific areas of structural weakness. By visualizing the stress concentrations and deformation patterns, it provided valuable insights into the modifications required to enhance the durability and stability of link 1, thereby ensuring the overall robustness of the robotic arm.

The redesigned component demonstrated a marked improvement in structural performance compared to the original design, particularly in terms of deformation reduction. This enhancement was evident in the subsequent analysis of the modified part, which confirmed a substantial increase in its structural integrity.

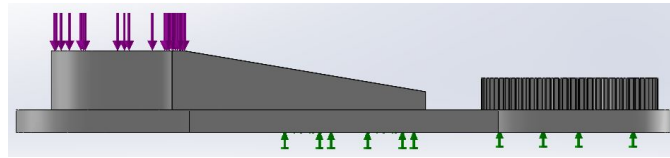


Figure 10. Re-designed piece.

The advanced design effectively minimized deformation, as can be clearly observed in Figure 11. This improvement was not only a testament to the robustness of the new design but also a confirmation that it successfully met the established structural performance criteria.

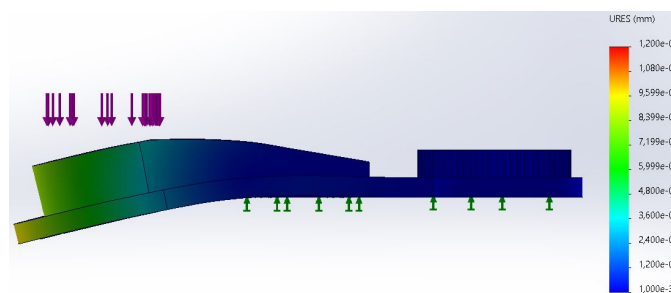


Figure 11. Deformation of the re-design.

As illustrated in Figure 10, the re-engineered link displayed significantly improved resilience under operational stress, showcasing the effectiveness of the design modifications. These changes were instrumental in ensuring the reliability and longevity of the robotic arm, marking a pivotal advancement in the project.

To facilitate a direct comparison between the original and redesigned parts, a force of 1.4 Newtons, equivalent to a load of 140 grams, was applied to the link connected to the gripper in both scenarios.

Following an exhaustive analysis, it became evident that replacing the original part with the modified design was the most effective solution. This decision led to the successful assembly of the complete robotic arm, as depicted in Figure 1.

This strategic intervention effectively addressed the previously identified issue, significantly enhancing the robotic arm's stability and operational efficiency. The replacement of the part marked a critical step in optimizing the robotic arm's functionality, ensuring its robust performance in practical applications.

1.5. Denavit-Hartenberg

This section shows the Denavit-Hartenberg parameter table, a key tool in the analysis and kinematic modeling of the robotic arm [10]. These parameters, such as link lengths, offset angles, and center distances, allows to accurately describe the geometry and relationship of motion between the links of the arm. Its correct determination is essential to achieve precise and efficient control of the gripper positions and orientations during packaging tasks.

Below is the arrangement of the reference frames in the robot, in Figure 12. Reference frames are coordinate systems used to describe the position and orientation of each link in the robotic arm. These frames are essential to perform the calculations of kinematics and control of the robot. By properly assigning the reference frames, the trajectory and configuration of the arm in the work space can be accurately determined. This information is essential to achieve coordinated and precise movements of the gripper during packaging tasks.

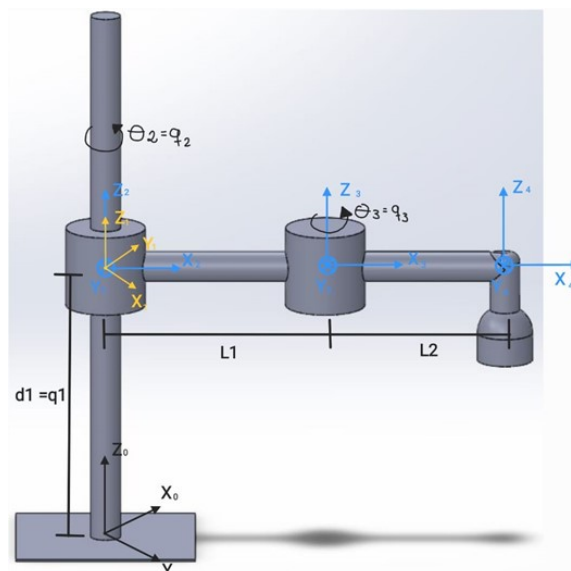


Figure 12. Frames positions.

Below in Table 6 the Denavit-Hartenberg-Parameters (DHP) for the PRR robot is presented. These parameters describe the geometry and the relationship between the different links of the robot.

Table 6. Denavit-Hartenberg Parameters.

i	α_{i-1}	a_{i-1}	d_i	θ_i
1	0	0	0	q_1
2	0	0	q_2	0
3	0	L_1	q_3	0
4	0	L_2	0	0

The homogeneous transformation matrix shown below represents the position and orientation of the gripper in three-dimensional space. These results obtained using Matlab, are fundamental for the control and planning of the robot's movements, ensuring a precise and efficient operation in the manipulation of objects.

$$\begin{bmatrix} \cos(\theta_1 + \theta_2) & -\sin(\theta_1 + \theta_2) & 0 & 13 \cos(\theta_1 + \theta_2) + 14 \cos(\theta_1) \\ \sin(\theta_1 + \theta_2) & \cos(\theta_1 + \theta_2) & 0 & 13 \sin(\theta_1 + \theta_2) + 14 \sin(\theta_1) \\ 0 & 0 & 1 & d_3 \\ 0 & 0 & 0 & 1 \end{bmatrix}$$

1.6. Jacobians Matrix

In this section, the equations and derivations of the Jacobian matrix for the PRR robot is presented. The Jacobian matrix plays a crucial role in the kinematics of the robot, since it relates the speeds of the actuators with the linear and angular speeds of the gripper [11]. In this case, a 2x2 Jacobian matrix was opted, since the positioning angle is not a determining factor for the main objective of placing the chocolates in their precise location.

By considering a 2x2 Jacobian matrix, it focus on capturing and calculating only the essential components for the packaging process. Since the objective is focused on the precise placement of the chocolates and not on the exact angular orientation, simplifying the Jacobian matrix allows to optimize and speed up the calculation of the required velocities. With this results obtained in Matlab, it guarantees efficient and precise control of the robot's movement, ensuring smooth and successful handling of the chocolates during the packaging process. This matrix can be seen below.

$$\begin{bmatrix} -13 \sin(\theta_1 + \theta_2) - 14 \sin(\theta_1) & -13 \sin(\theta_1 + \theta_2) \\ 13 \cos(\theta_1 + \theta_2) + 14 \cos(\theta_1) & 13 \cos(\theta_1 + \theta_2) \end{bmatrix}$$

1.7. Task-Space

Task-space, often referred to as the operational space, is the physical area within which the end-effector (in this case, the gripper of the robotic arm) performs its tasks [12]. This space is defined by the positions that the end-effector can reach and the orientations it can achieve during operation. For a SCARA robot, which is primarily designed for planar movements, the task-space would typically be a two-dimensional area at a fixed height from the base, resembling a disc-shaped region where the robot can manipulate objects.

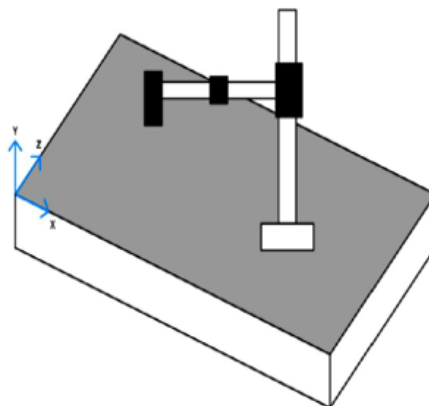


Figure 13. Task-space of the PRR robot.

1.8. C-Space

Configuration space, or C-space, represents the complete set of possible positions of the robot's joints. For a SCARA robot, which typically has two parallel rotary joints to control the arm and a prismatic joint for vertical movement, the C-space can be visualized as a three-dimensional volume where each dimension corresponds to one of the joints degrees of freedom [13]. Understanding the C-space is critical for planning the robot's motion, as it helps in determining how the joints should move to reach a particular point in the task-space.

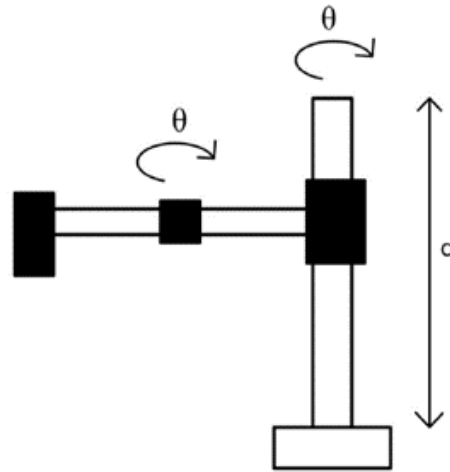


Figure 14. C-space of the PRR robot.

1.9. Work-Space

The work-space of a robot is the physical volume that encompasses all the points that the robot's end-effector can reach, considering the full range of motion of every joint. Unlike the task-space, which is usually defined for a specific task and orientation, the work-space includes all possible configurations and orientations of the end-effector. In the context of a SCARA robot, the work-space would include not only the two-dimensional task-space but also the vertical movements allowed by the prismatic joint. [14]

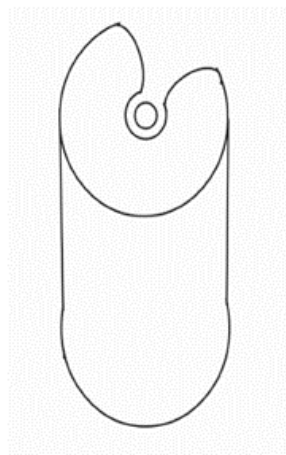


Figure 15. Work-Space of the PRR robot.

Each of these spaces plays a crucial role in the kinematics and control of robotic systems, enabling precise positioning and maneuvering within the robot's environment.

2. Electronic design

In this section, the electronic components used in the project and its characteristics with their corresponding functionalities within the project will be explained.

2.1. Component selection

The electronic design of the robotic arm required careful consideration and selection of components to ensure seamless integration and optimal performance. The primary objective was to achieve precise control, reliable movement, and efficient operation of the arm. The electronic drawings for this project can be found in appendix B.

2.2. Micro-Controller

An Arduino Uno board (Figure 16), was chosen as the micro-controller due to its versatility, ease of use, and wide community support. Its compatibility with various sensors and actuators, along with its ability to handle multiple inputs and outputs simultaneously, made it an ideal choice for this project.

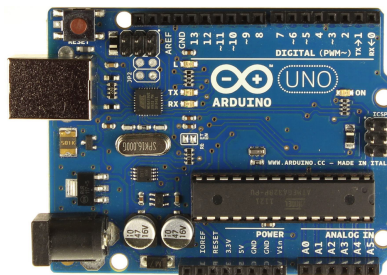


Figure 16. Arduino Uno board.

[15]

2.3. 5v Relay module

An integral part of the robotic arm's design was the inclusion of a 5V relay module (Figure 17), which played a crucial role in the operation of the vacuum pump. The vacuum pump, in turn, was a key component for the arm's Universal Vacuum Grip (UVG), enabling it to pick up and handle chocolates with precision.

The 5V relay module was selected for its ability to act as an electrically operated switch. It allowed the Arduino control board to safely and efficiently control the higher power

vacuum pump, which operates at a voltage and current beyond the direct handling capacity of the Arduino. This module effectively bridged the gap between the low-power control signals from the Arduino and the high-power requirements of the vacuum pump.



Figure 17. 5v Relay module.
[16]

The use of the relay module ensured safe operation, as it isolated the control circuitry from the power circuit, minimizing the risk of electrical hazards. It also provided the flexibility to switch the vacuum pump on and off based on the robotic arm's operational needs, and its ability to handle the power requirements of the vacuum pump, ensured a seamless integration between the processes.

2.4. Vacuum Pump

The vacuum pump (Figure 18), was a critical component for the UVG system of the robotic arm. It created the necessary vacuum to securely grip the chocolates without damaging them. The pump was chosen for its reliability, adequate suction power, and low power requirements as it only is a 12v DC Motor air pump.



Figure 18. 12v DC Motor Mini Air Pump.
[17]

The vacuum pump's operation was meticulously synchronized with the arm's movements. When the arm positioned itself over a chocolate, the pump was activated to grip the chocolate. Once the chocolate was securely held, the arm moved to place it in the designated slot on the tray. After successful placement, the pump was deactivated to release the chocolate.

2.5. Motors and drivers

Three NEMA-17 (Figure 19) motors were used in the project and they have a maximum current rating of 2.5A, although they are typically operated at 1 or 1.5A. To control these motors, an A4988 driver (Figure 20) was utilized. This driver is capable of delivering a current of 2A per coil. With the NEMA-17 motor's default step count of 200 steps per revolution, a resolution of 1.8 degrees per step was achieved.

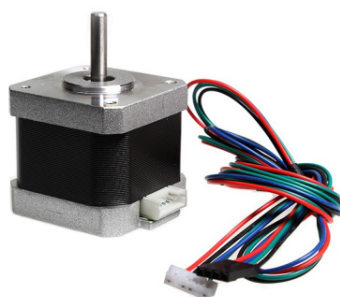


Figure 19. NEMA-17 motor.
[18]

However, by employing the A4988 driver, a finer resolution can be achieved. The A4988 driver offers a maximum resolution of 16 micro-steps. This means that the NEMA-17 motor can now take 3200 steps per revolution, resulting in a reduced step size of 0.1125 degrees per step. This enhanced resolution enables smoother and more precise control of the motor's movements, allowing for intricate and accurate positioning in the robotic arm system.

It is important to set the current limit of the driver appropriately to ensure optimal motor performance. The current limit should be lower than the rated current of the motor to prevent overheating. However, it is crucial to find the right balance, as setting the current too low may result in lost steps and compromised precision.

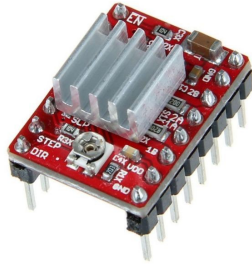


Figure 20. A4988 driver.
[19]

By leveraging the capabilities of the NEMA-17 motors and A4988 driver, a desired level of control and precision could be achieved in the project, enabling smooth and accurate motion of the robotic arm.

2.6. CNC-Shield

The CNC-Shield V3 (Figure 21) is an expansion module specifically designed for CNC machines, such as engraving or 3D printers. It serves as a vital component in the project, providing additional functionality and control. The shield operates on a 12V power supply, which aligns with the voltage requirement of the power source. One of the key features of the Shield V3 is its capacity to accommodate up to 4 drivers. These drivers play a crucial role in regulating the current flowing to the motors. Each driver is equipped with a small adjustment potentiometer, allowing to fine-tune the current limit. In this case the A4988 driver was used as it was mentioned before.

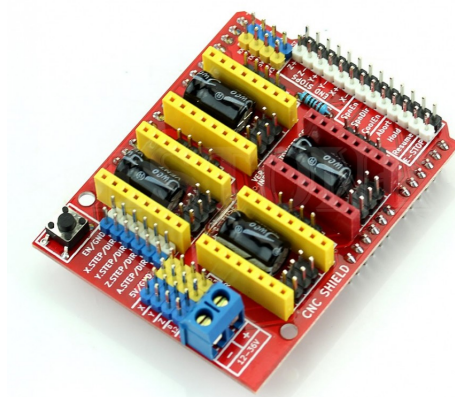


Figure 21. CNC-Shield.
[20]

2.7. Camera

Another key component in the project, was the Vmax 1080P camera (Figure 22), which played a crucial role in the object detection and quality control aspects of the project. The camera's characteristics were carefully selected to ensure optimal performance in these tasks.



Figure 22. Vmax Full HD Webcam.
[21]

The camera boasted a Full HD 1080P resolution, providing clear and detailed images necessary for accurate object detection and analysis. This high-resolution imaging was essential in distinguishing between different types of chocolates, such as the gold-wrapped Ferrero Rocher and the white-wrapped Raffaello chocolates, and ensuring their correct placement in the packaging trays. The viewing angle of 90° allowed for comprehensive monitoring of the workspace, ensuring that the entire area where the chocolates were placed and picked up was within the camera's field of vision.

2.8. Power supply

A 12V-5A power supply was employed for supplying the three NEMA-17 motors. With the help of the A4988 driver, each NEMA-17 motor needed only 1.3 A approximately in order to power up. Therefore the power supply selected was more than enough. Other electronic components such as the Arduino Uno board, relay module and webcam aren't considered here because they are powered up when connected to the computer.

2.9. Electronic block diagram

The electronic block diagram that resumes the previous section is shown in Figure 23.

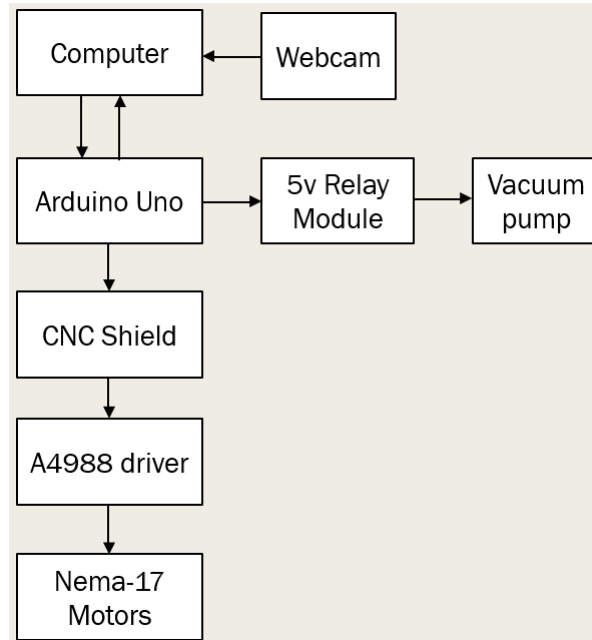


Figure 23. Electronic block diagram.

3. Programming

This section is designed to provide a comprehensive understanding of the various programming strategies, tools, and techniques employed to bring this innovative project to life. The Arduino program that is in charge of the movements of the stepper motors and the 5v relay module that controls the vacuum pump. Then two Python programs were developed for controlling the robotic arm, managing object detection, and facilitating user interactions through the graphical user interface (GUI). The choice of Python, known for its simplicity and robust libraries, significantly contributed to the efficient and effective development of the project.

3.1. Arduino Program

The program accepts serial commands from an external source (User Interface) and translates these commands into physical motion of the robot. The program expects a sequence of three integers, which correspond to the desired positions (angles or linear displacement) for each of the robot's three axes.

When Arduino receives these values, it maps them to the appropriate range for each stepper motor. It then commands each motor to move to the specified position. Regarding the relay, when the arduino receives the activation commands from the python interface it sets the relay into a HIGH state if the Relay On button was pressed. If the relay of button was pressed it sets the relay to a LOW state.

In addition to movement, the Arduino program also supports calibration of the robot's axes and gripper. Upon startup, it will move each axis to a known home position and start with the vacuum pump off. This ensures that subsequent commands are executed accurately, relative to this initial position.

Furthermore, the Arduino program contains logic to ensure the received commands are valid and safe for the robot to execute. The flowchart of this program can be seen in Figure 24.

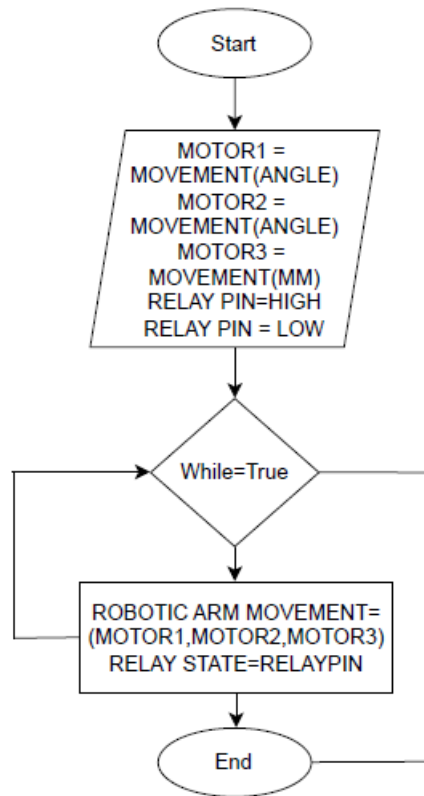


Figure 24. Flowchart Arduino program.

The Arduino program controls the physical aspects of the robot, directly interfacing with the robot's actuators. When it receives a command over serial communication from the user interface, it decodes the command and moves the robot to the specified position or activates the vacuum pump depending on the command received.

3.2. Object Detection program

A distinctive feature of this project is the integration of object detection, achieved with the implementation of a pre-trained YOLO (You Only Look Once) model [22]. This model operates as part of a dedicated computer vision system, tasked with identifying and categorizing chocolates in real-time.

The object detection mechanism is dependent on a camera that continuously captures images of the workspace. These images are processed by the YOLO model to detect and classify chocolates into predetermined categories which in this case are two. Class 'White' and class 'Gold'.

The YOLO model, specifically the YOLO V8 version, functions as the backbone of the object detection system. It's renowned for its real-time processing capabilities [23], crucial for the dynamic environment of the chocolate packaging process. The model identifies chocolates and their respective positions by analyzing each image and calculating coordinates based on the bounding boxes it generates. The flowchart of this program can be seen in Figure 25. This information is crucial in guiding the robotic arm to the correct pickup and drop-off points.

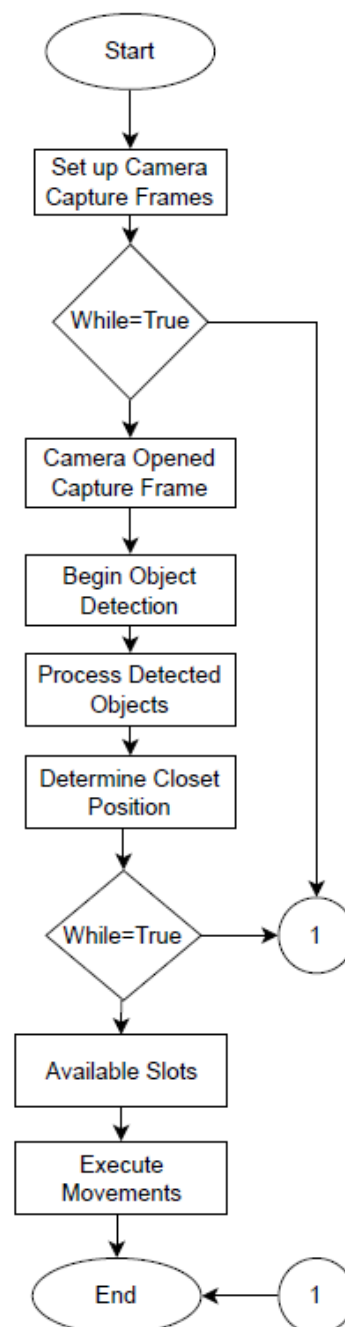


Figure 25. Flowchart Object detection program.

Communication between the object detection system and the robotic arm is key to the project's success. The system relays information about detected chocolates, including their type and position, to the arm's control system. Based on the user's chosen configuration and the identified type of chocolate, the arm maneuvers to pick up and place the chocolate in the designated slot on the tray. This process is repeated until all chocolates are sorted or until the user intervenes to stop the operation.

The integration of advanced computer vision and artificial intelligence significantly enhances the capabilities of the robotic arm. The YOLO model, central to the object detection system, has been trained to recognize different types of chocolates. This training makes the model adept at handling various shapes and sizes of chocolates, adapting to different arrangements on the fly. Implementing AI and computer vision into the robotic arm transforms it from a simple mechanical device to an intelligent system capable of making real-time decisions. This adaptability is crucial for a process like chocolate packaging, where variations are common. Moreover, the AI system continually learns from its environment, improving its detection accuracy over time and ensuring the reliability of the packaging process.

One of the challenges in implementing AI was ensuring consistent detection accuracy under different lighting conditions and varying orientations of chocolates. To overcome this, the YOLO model underwent fine-tuning and optimization specifically for chocolate detection. Additionally, size filters were implemented to minimize false positives, such as mistakenly identifying the bases as chocolates.

3.3. Graphical User Interface (GUI)

The user interface program creates a GUI using the Tkinter library [24], providing a graphical interface for controlling and interacting with the robotic arm system. It facilitates manual adjustment of one linear Z joint and two rotational joints using sliders. It provides buttons for saving positions, executing sequences automatically, and controlling the gripper. The interface offers an intuitive way to operate the system and mon-

itor its status through a status label and a listbox displaying the saved configurations. The interface also enables the activation and deactivation of the relay controlling the vacuum pump, which is an integral component of the gripper. Additionally, it features an automatic mode, allowing for the continuous cycling through a series of pre-recorded positions, thereby facilitating seamless and repetitive operations. These GUI can be seen in (Figure 26).

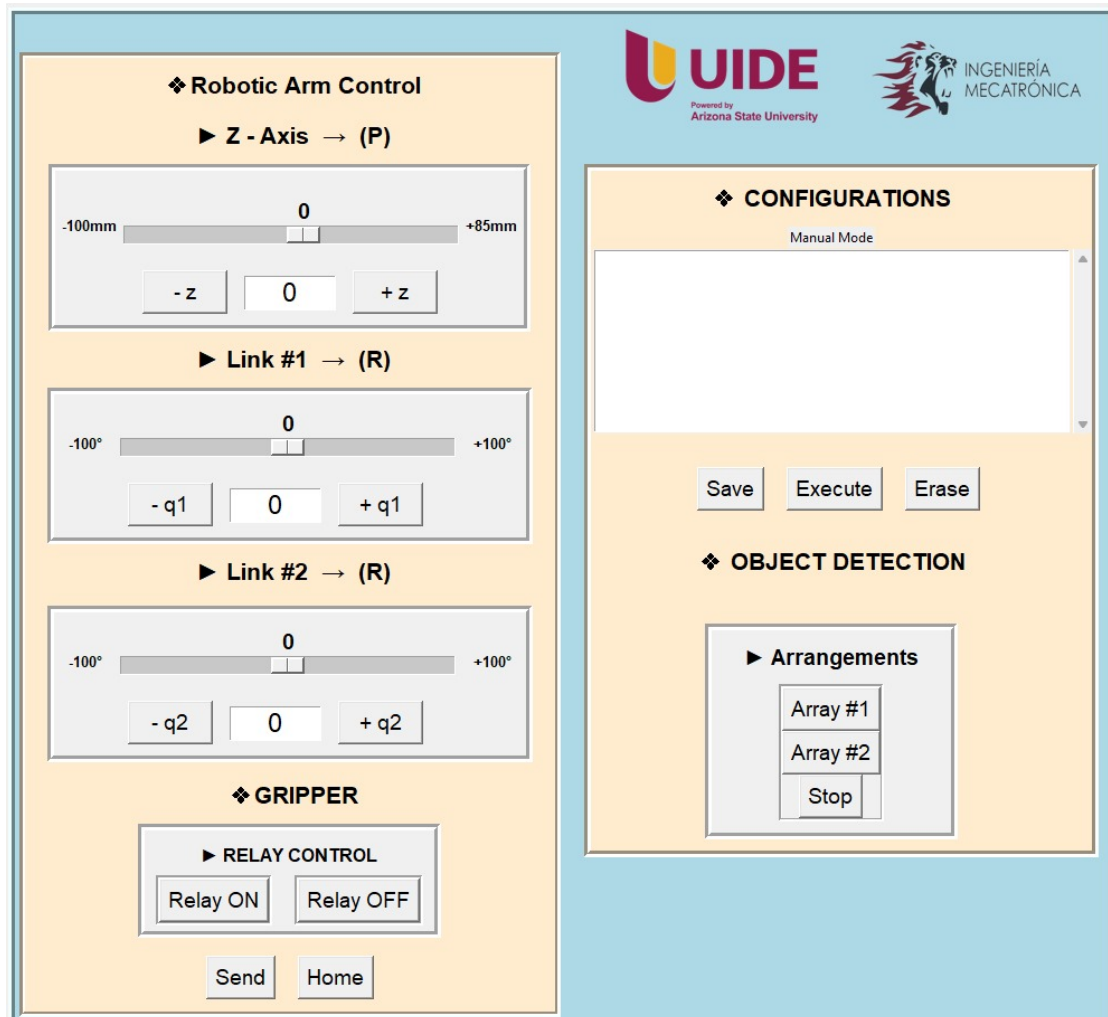


Figure 26. Graphical User Interface developed.

Additionally, it facilitates the initiation of the automated packaging process that uses the object detection algorithm with the use of three buttons. Two of them are for establishing different configurations, empowering users to direct the arm to sort chocolates into pre-set patterns based on their selection and a stop button that halts the object detection when the process has finished or other aspects of the GUI have to be used. The flowchart of this program can be seen in Figure 27.

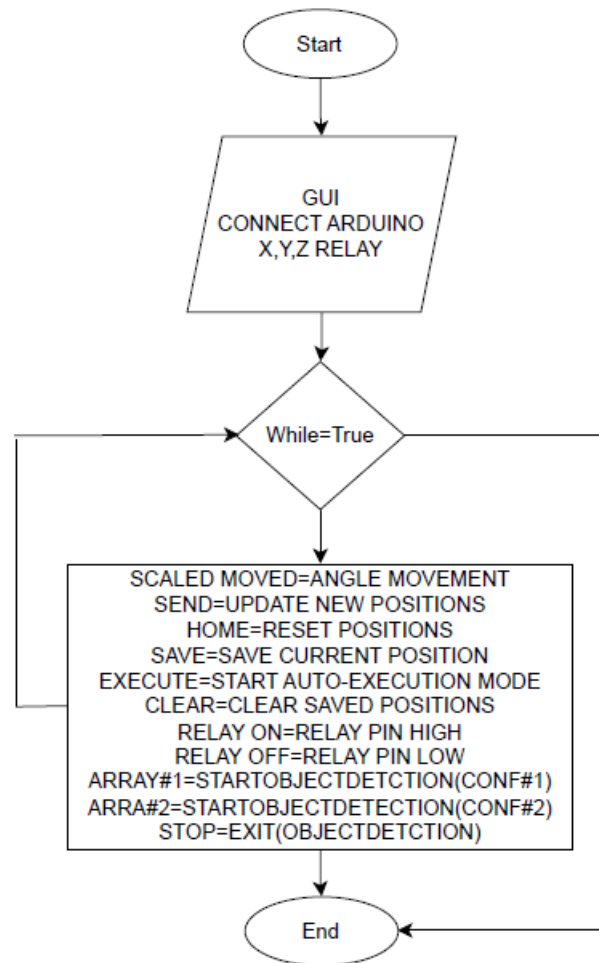


Figure 27. Flowchart User Interface program.

The program communicates with the Arduino board using serial communication via the pyArduino library. This library handles both the sending of commands from the Python program to the Arduino board, and the reading of data from the Arduino board back to the Python program.

3.4. Dataset

The creation of a custom dataset played a crucial role in the successful implementation of artificial intelligence for the chocolate packaging robotic arm. In total, 1920 images were meticulously compiled to train, validate, and test the object detection model.

The dataset was divided into 1680 training images (88%), 160 validation images (8%), and 80 test images (4%), ensuring a comprehensive foundation for robust model training. An example of how the images were taken can be seen in (Figure 28).

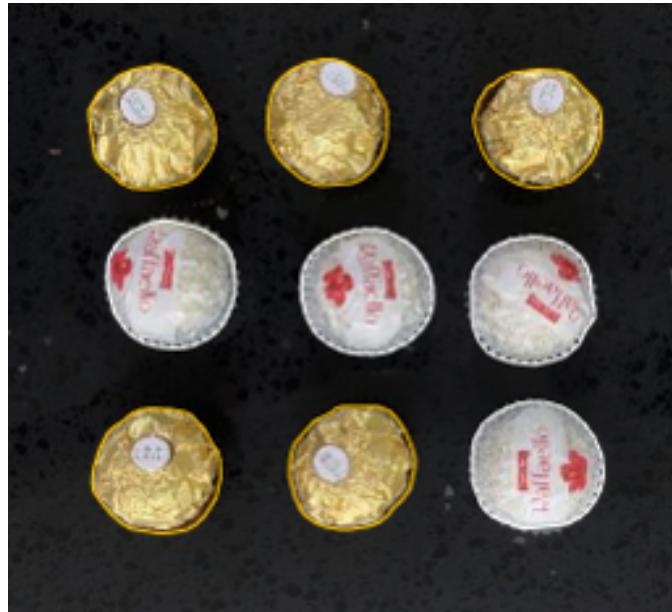


Figure 28. Images taken for training.

Two distinct classes were identified for the dataset: 'White' and 'Gold' (Figure 29). The 'Gold' class encapsulated images of Ferrero Rocher chocolates, renowned for their signature golden wrappers, while the 'White' class consisted of Raffaello chocolates, recognizable by their white, coconut-dusted appearances. This categorization was pivotal in enabling the YOLO model to differentiate between the two types of chocolates with high precision.



Figure 29. Classes created for detection.

Photography for the dataset was conducted using an iPhone 11, ensuring high-quality image capture [25]. To maintain consistency and optimize the model's performance, each image was resized to a fixed dimension of 640x640 pixels. This uniformity in image size played a critical part in standardizing the input for model training.

The process of labeling the images was facilitated by Roboflow [26], a robust tool that streamlined the annotation of chocolate types and their positions within each image. Following the labeling phase, the model training was initially executed on Google Colab [27], taking around 3 hours and 45 minutes. However, by upgrading to Colab Pro and leveraging more powerful TPUs (Tensor Processing Units), the training duration was significantly reduced to just 52 minutes (Figure 30), showcasing the efficiency gains from using advanced computational resources.

```
50 epochs completed in 0.524 hours.
Optimizer stripped from runs/detect/train/weights/last.pt, 52.0MB
Optimizer stripped from runs/detect/train/weights/best.pt, 52.0MB

Validating runs/detect/train/weights/best.pt...
Ultralytics YOLOv8.0.196 Python-3.10.12 torch-2.1.0+cu121 CUDA:0 (Tesla V100-SXM2-16GB, 16151MiB)
Model summary (fused): 218 layers, 25840918 parameters, 0 gradients, 78.7 GFLOPs
  Class      Images  Instances  Box(P)      R      mAP50  mAP50-95): 100% 5/5 [00:03<00:00, 1.52it/s]
  all        160     518       0.993      0.986   0.99   0.957
  Blanco     160     256       0.99       0.984   0.988  0.954
  Dorado     160     262       0.996      0.989   0.992  0.959
Speed: 0.1ms preprocess, 12.9ms inference, 0.0ms loss, 3.3ms postprocess per image
```

Figure 30. Training Time.

A series of augmentation techniques were employed to enhance the diversity of the training dataset (Table 7). These included rotations, shearing, adjustments in brightness, noise, blur, and exposure variations. Such augmentations simulated different real-world conditions, preparing the model to handle various lighting and orientation scenarios encountered during the actual packaging process.

Augmentation Type	Range/Description
90° Rotate	Clockwise, Counter-Clockwise, Upside Down
Rotation	Between -15° and +15°
Shear	±15° Horizontal, ±15° Vertical
Brightness	Between -30% and +30%
Exposure	Between -25% and +25%
Blur	Up to 2.5px
Noise	Up to 5% of pixels

Table 7. Summary of Image Augmentation Techniques

After training the model for 50 epochs, an impressive precision of 99.4% and a recall of 98.6% were achieved. It was determined that extending the training beyond 50 epochs led to overfitting, where the model performs exceptionally well on the training data but

lacks generalization to new, unseen data. The chosen epoch count struck a balance between learning the necessary features and avoiding overfitting, resulting in a model that is both accurate and generalizable (Figure 31).

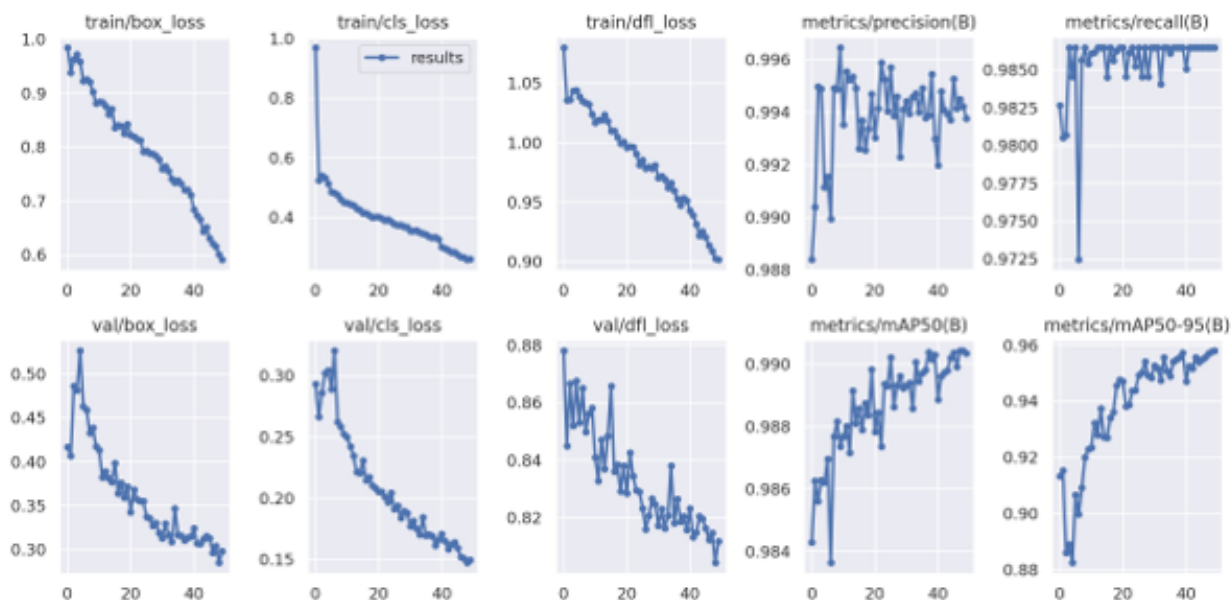


Figure 31. Training Results charts.

3.5. Confusion Matrix

The confusion matrix displays the performance of the classification model for identifying chocolates (Figure 32). The matrix shows three classes: 'White', 'Gold', and background, suggesting that the model is classifying chocolates into two categories (White and Gold) and identifying instances where no chocolate is present (background).

For the White class, the model has a very high true positive rate, as indicated by the value of 0.98 on the diagonal. This means that 98% of the time, the model correctly identifies White chocolates. The 'Gold' class also exhibits a high true positive rate, with a value of 0.99 on the diagonal, meaning the model correctly identifies Gold chocolates 99% of the time.

The background class has low values (0.02 and 0.01) in the corresponding 'White' and 'Gold' columns, respectively. These represent the instances where the model incorrectly identifies a background as either 'White' or 'Gold', which is very rare. There is

a 50-50 split in the off-diagonal elements between 'White' and 'Gold', which suggests that when a mistake is made, the model is just as likely to misclassify a 'White' as a 'Gold' and vice versa.

The model demonstrates high precision and accuracy in classifying 'White' and 'Gold' classes, the relatively high number of True Positives for both 'White' and 'Gold' suggests that the model is very effective for these classes.

The balance in misclassification between 'White' and 'Gold' when the true class is 'Background' suggests that the model may have difficulty distinguishing 'Background' features that are similar to those of 'White' and 'Gold'.

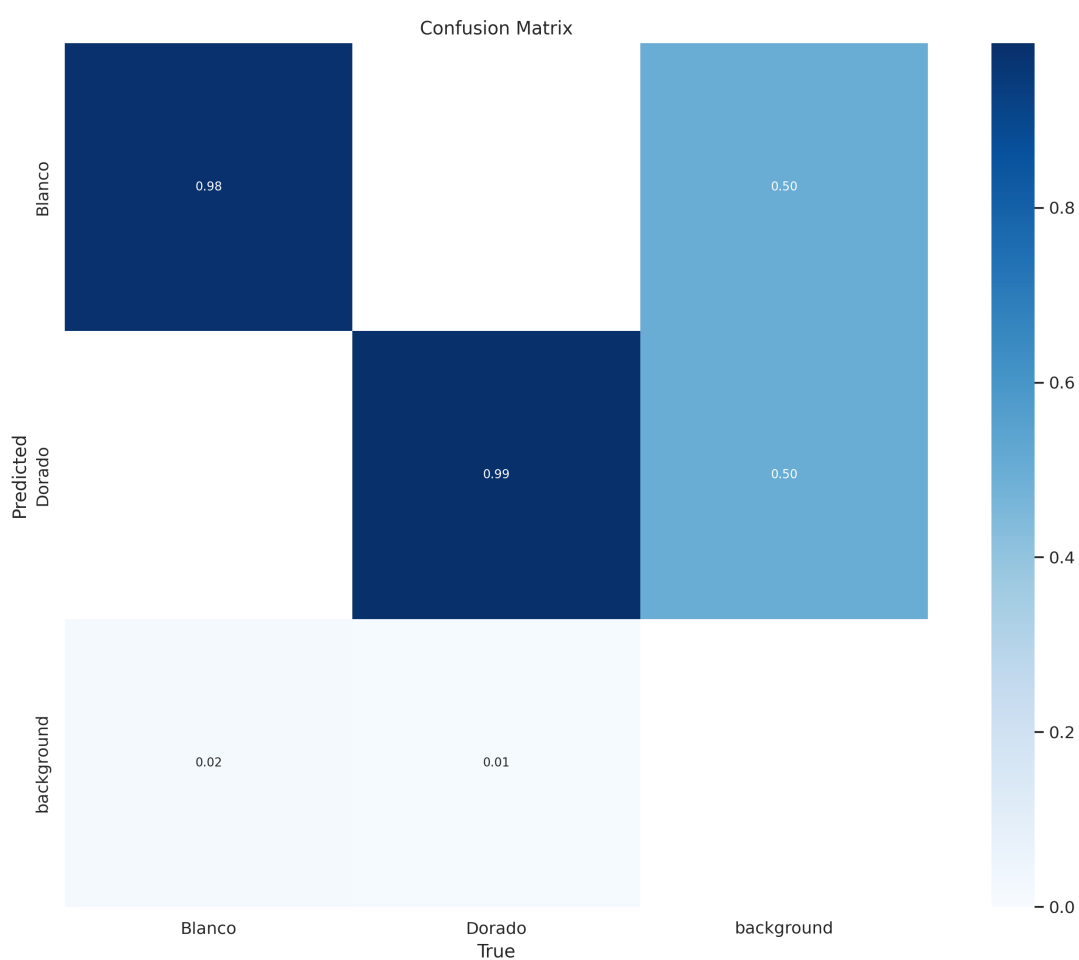


Figure 32. Confusion matrix obtained.

4. Tests & Results

In the testing phase of the project, two distinct evaluation methods were employed to validate the performance of the object detection algorithm. The first method involved static images of chocolates, which were part of the validation set not seen by the model during training (Figure 33). These images were crucial in determining the model's accuracy in a controlled environment. The algorithm demonstrated high confidence levels, consistently registering values of 0.95 and above, indicating a robust ability to recognize and classify chocolates correctly based on the learned features.



Figure 33. Images tested.

The second testing method shifted from static analysis to dynamic, real-world conditions, utilizing the camera in real-time to identify chocolates as they appear in the operational environment. During these live tests, the model successfully recognized and classified chocolates with lower confidence scores, averaging around 0.84 (Figure 34).

This decrease in confidence, compared to the static image tests, is not uncommon in machine learning applications due to the increased complexity and variability present in live scenarios, such as changes in lighting, orientation, and background. Despite the lower confidence scores in live testing compared to the validation images, the model's ability to accurately identify chocolate types in real time is a testament to its practical

applicability. The real-time test outcomes are essential for understanding the model's operational performance and provide insights into its reliability under typical use conditions. These findings demonstrate the model's proficiency and validate its integration into the chocolate packaging system, ensuring that it can perform reliably in a live production setting.



Figure 34. Real time view testing.

A total of 20 practical tests were performed with the purpose of analyzing the performance of the prototype. The results obtained offer a variety of scenarios that highlight the effectiveness of the project and the time it takes to finish a configuration. These tests were divided into two sections.

Under controlled lighting conditions, a series of ten tests were conducted using a consistent and stable source of white light. This light source was positioned at the top of the room, angled in such a way that it did not cast direct light on the chocolates or the camera at the commencement of the object detection and the automated sorting process. In this controlled environment, the algorithm delivered flawless performance, accurately identifying the different types of chocolates irrespective of their positions. This precise detection allowed the robotic arm to correctly allocate each chocolate to its designated slot, in accordance with the pre-selected configuration.

The success of these tests can be attributed to the stable lighting conditions, which eliminated the occurrence of incorrect detections that could potentially disrupt the accurate classification of the chocolates. The results of these tests, demonstrating the effectiveness of the object detection under fixed light conditions, are detailed in Table 8.

Table 8. Results under controlled Lighting Conditions

# Tests	Total Time (min)		Correct Detection		Correct Placement	
	Array#1	Array#2	Array#1	Array#2	Array#1	Array#2
1	3:00	3:02	4	4	4	4
2	2:58	2:59	4	4	4	4
3	2:59	3:03	4	4	4	4
4	3:01	2:59	4	4	4	4
5	3:02	2:58	4	4	4	4
6	3:00	3:01	4	4	4	4
7	2:59	3:00	4	4	4	4
8	2:58	3:02	4	4	4	4
9	3:00	3:01	4	4	4	4
10	3:01	2:59	4	4	4	4
Avg	2.83 min	2.84 min	4	4	4	4

In a contrasting set of conditions, ten tests were conducted under variable lighting to evaluate the robustness of the object detection algorithm and the automated sorting process. Unlike the previous fixed lighting scenario, the light in this environment was not constant, which introduced a level of complexity to the detection task. The source of light, subject to change, was not directly above the chocolates and the camera, it was natural light that came from open spaces such as windows or open doors, creating diverse shadows and highlights during the tests.

The results, as shown in Table 9, indicate a notable variance from the perfect outcomes observed in the fixed lighting setup. Although the algorithm still managed to identify the types of chocolates with a reasonable degree of accuracy, there were instances where the detection and subsequent sorting did not match the ideal performance. The robotic arm's precision in allocating chocolates to their respective slots was affected by these lighting variations, leading to a slight drop in the consistency of correct placements and detections.

Table 9. Results under Variable Light Conditions

# Tests	Total Time (min)		Correct Detection		Correct Placement	
	Array#1	Array#2	Array#1	Array#2	Array#1	Array#2
1	3:02	2:58	3	3	3	3
2	2:59	2:59	4	3	4	3
3	2:58	3:03	3	2	3	2
4	3:01	3:01	3	3	3	3
5	3:02	3:00	4	3	4	3
6	3:00	2:58	2	4	2	4
7	2:59	3:01	3	3	3	3
8	3:00	3:00	4	3	4	3
9	3:00	3:01	4	4	4	4
10	3:01	2:59	3	3	3	3
Avg	2.88 min	2.85 min	3.3	3.1	3.3	3.1

During these tests, it was also observed that variations in time between different configurations are minimal, attributed to the fact that movement speeds and time delays in the operations, including relay activation's, are maintained as constant.

The robotic arm is programmed not to initiate its task if no chocolates are detected at the outset of the process. For the system to start effectively, chocolates must be accurately positioned; otherwise, the arm will default to the last known location of the intended chocolate class should detection cease mid-process.

The effectiveness of the object detection, which correlates directly with the accuracy of chocolate placement, was high under fixed lighting conditions, with the algorithm flawlessly identifying the type of chocolate and its position without errors. However, performance declined under variable lighting, suggesting that a controlled lighting environment is crucial for the robotic arm's accuracy in task execution.

This recommendation is to ensure that the system operates without discrepancies that could affect its functionality. Also its important to state that setting up the camera in a correct position, assuring the chocolates are within the view of the camera, before starting the object detection process in order to avoid issues on the detecting process.

If Array 1 button is pressed, the configuration in which the chocolates are going to be arranged is shown in figure 35.



Figure 35. Array 1.

If Array 2 button is pressed, the configuration in which the chocolates are going to be arranged is shown in figure 36.



Figure 36. Array 2.

Table 10, captures the performance of the end effector (UVG), which molds to the shape of the object it is picking up, in this case, chocolates. During the test, the UVG was tasked with picking up a series of ten chocolates to assess its efficacy over multiple cycles. The results indicated that the gripper successfully picked up the first eight chocolates. However, by the ninth chocolate, the balloon had lost its adaptive shape, leading to a decline in grip strength and the inability to successfully lift the chocolates.

Table 10. End Effector Performance Test Results

# Chocolates	Picked Up Successfully	Failed to Pick Up
Chocolate #1	✓	
Chocolate #2	✓	
Chocolate #3	✓	
Chocolate #4	✓	
Chocolate #5	✓	
Chocolate #6	✓	
Chocolate #7	✓	
Chocolate #8	✓	
Chocolate #9		X
Chocolate #10		X

After eight consecutive uses, the UVG requires reconfiguration. The optimal solution identified to enhance the gripper's performance involves the installation of a secondary pump. Unlike the primary pump which evacuates air to form the grip shape, this second pump would introduce air back into the balloon upon the release of a chocolate. This action would not only aid in releasing the chocolate into its designated slot but also ensure that the balloon returns to its original shape, ready to adapt to the next chocolate. Implementing this solution would theoretically allow for unlimited operational cycles without a loss in the gripper's performance.

5. Total Costs

Table 11 presents the cost breakdown of the mechanical and electronic components required for the development of both the Arm and the gripper. The table provides detailed information regarding the expenses associated with each element, enabling a comprehensive understanding of the budget allocation for this project. By analyzing these costs, it becomes possible to assess the financial investment required for the construction and assembly of the robotic system. The data presented in the table will serve as a valuable reference for future budget planning and resource allocation in similar projects. In this case the total cost for making the project is of \$795 US-Dollars.

Table 11. Total Costs

Product	Quantity	Unit Cost	Total
Arduino Uno	1	10.75	10.75
Power supply 12V 5A	1	10	10
Shield CNC for Arduino UNO	1	5	5
Driver A4988	3	7.5	22.5
Nema 17 Motor	3	12.5	37.5
Female plug for power supply	1	0.50	0.50
Linear bearing lm8uu	6	2.5	15
Bearing 15x32x9	3	6	18
PLA and TPU	2	22	44
THSL screw and nut	1	1	13
Stainless steel rod 8mm	3	5.5	16.5
Toothed belt 20 teeth	2	3	6
Flexible coupling 5*8	1	3	3
Wires	2	2 per m	4
6Vdc 370 Air Mini Airpump	1	9.90	9.90
Hose	1	1 per m	1
Balloon	1	0.5	0.5
USB type A cable	1	3.95	3.95
Table 70cmx60cmx8mm	1	30	30
Box Chocolates 2x2 units	2	6.7	13.4
Webcam	1	21	21
Labor	1	5 per hour	535
Total			795

6. Conclusions

The object detection algorithm, at the heart of this robotic arm system, exhibits commendable performance in classifying two distinct chocolate types. With a precision rate of 99.4% and a recall of 98.6%, the system's accuracy in a controlled environment is beyond satisfactory. When deployed in a live feed scenario, the algorithm continues to show respectable efficacy, with confidence values fluctuating between 0.8 and 0.9, ensuring reliable performance across different operational configurations.

However, it's noteworthy that the algorithm's confidence can waver in variable lighting conditions. Despite this, the system's robustness allows for successful task completion, albeit with a slight impact on the confidence levels. This resilience is indicative of the advanced capabilities of the AI model and its underlying neural network.

The system's efficiency is further evidenced by its average configuration completion time of approximately 2.84 minutes. This consistency holds across various configuration types, underscoring the system's reliability and the effectiveness of its programming.

An essential consideration for the system's optimal performance is the camera's positioning. Prior to the initiation of any configuration process, meticulous adjustments and testing of the camera setup are imperative. This precaution ensures the avoidance of detection errors or mislabeling of chocolates, as the camera's orientation significantly influences the algorithm's detections and, consequently, the robotic arm's movements.

The results obtained from the end effector testing, provide valuable insights into the performance of the Universal Vacuum Gripper (UVG) used as the end effector in the project. Initially, the UVG showed a high level of effectiveness, successfully picking up the first eight chocolates.

This demonstrated its capability to adapt to the shape of the objects, ensuring a secure grip for effective lifting. However, a notable decline in performance was observed after the eighth cycle. The inability of the UVG to successfully lift the ninth and tenth chocolates can be attributed to the loss of the balloon's adaptive shape, which is critical for maintaining a strong grip.

This pattern of performance indicates that while the UVG is highly effective for a limited number of cycles, its efficiency diminishes with extended use without reconfiguration. The testing highlights a pivotal aspect of the UVG's design, the need for periodic resetting of the balloon to retain its gripping ability.

To address this limitation and enhance the UVG's operational capacity, the introduction of a secondary air pump is proposed. This innovative solution aims to re-inflate the balloon after each cycle, restoring its original shape and readiness for subsequent use.

The implementation of this secondary pump is expected to facilitate continuous and reliable operation of the UVG, allowing for unlimited operational cycles without a compromise in performance. Thus, these test results not only affirm the UVG's initial effectiveness in automated chocolate handling but also illuminate the path for significant improvements, enhancing its longevity and reliability in automated food packaging processes.

In conclusion, the project has successfully demonstrated the practical application of AI in automating a complex task like chocolate packaging. The data-driven conclusions drawn from the system's performance underpin the potential for its application in various production environments, highlighting the importance of environmental control for AI-driven systems. The future of manufacturing, characterized by the integration of AI and robotics, appears promising, with the potential for significant advancements in operational efficiency, reliability, and quality assurance.

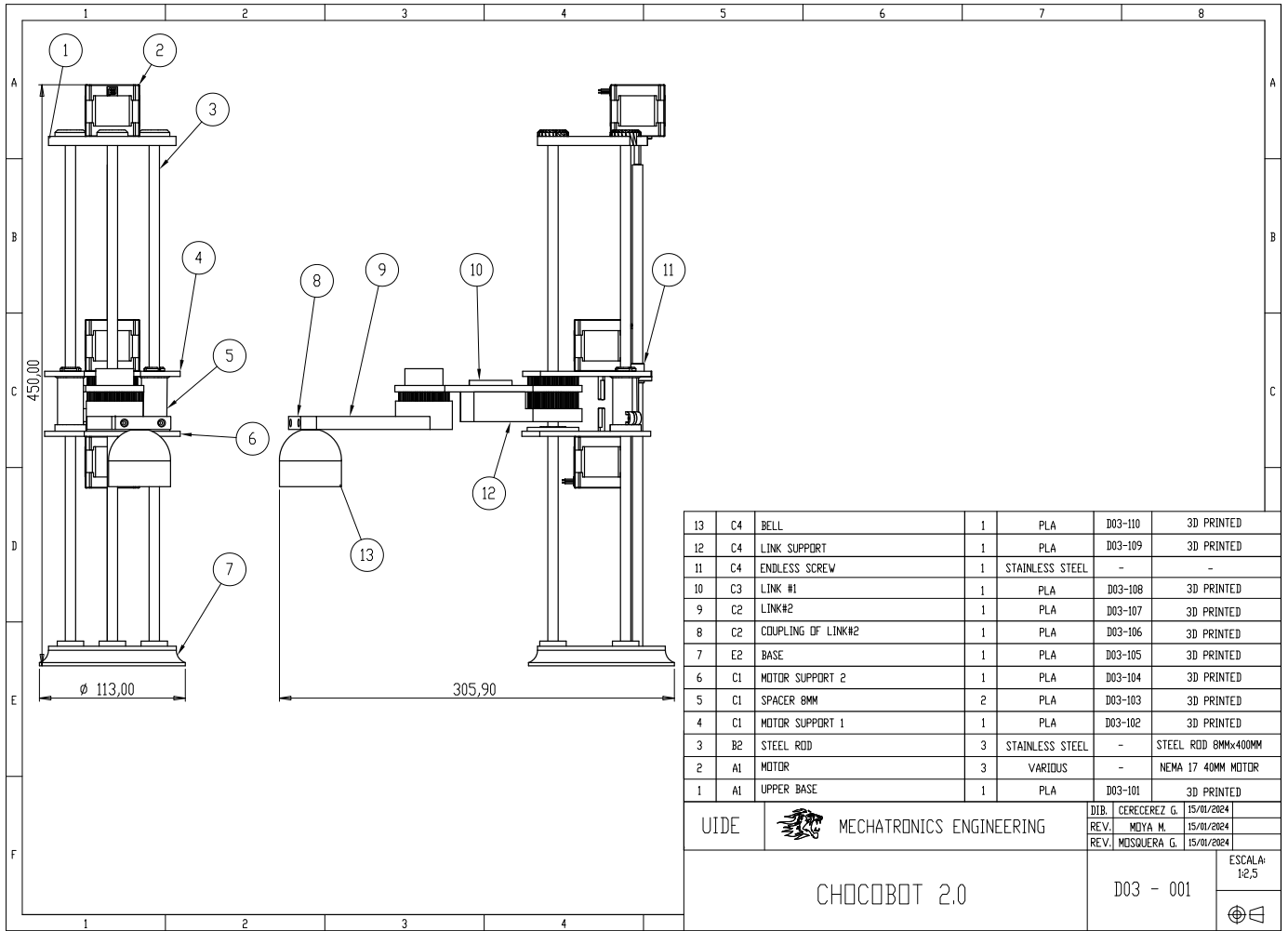
REFERENCES

- [1] F. Rocher, “Ferrero rocher,” 2021. [Online]. Available: <https://www.ferrerorocher.com/us/en/our-products/ferrero-rocher/3-piece-pack>
- [2] A. K. J. B. Kumar y B. Kumar, “Vacuum cup grippers for material handling in industry,” *nternational Journal of Science Technology*, pp. 1–8, 2017. [Online]. Available: <https://www.researchgate.net/profile/Binay-Kumar-8>
- [3] Festo, “vacuum technology principles.” [Online]. Available: <https://www.festo.com/net/SupportPortal/File/2868/BasicVacuumTechnologyPrinciples.pdf>
- [4] T. Chen, “Universal vacuum gripper (uvg) for efficient food packaging,” *IEEE Transactions on Robotics*, vol. 25, no. 3, pp. 78–85, 2020.
- [5] TWI, “What is pla? everything you need to know,” 2024. [Online]. Available: <https://www.twi-global.com/technical-knowledge/faqs/what-is-pla>
- [6] SpecialChem, “Comprehensive guide on thermoplastic polyurethanes (tpu),” 2024. [Online]. Available: <https://omnexus.specialchem.com/selection-guide/thermoplastic-polyurethanes-tpu>
- [7] K. S. Gears, “Design shapes of spur gears,” 2021. [Online]. Available: <https://khkgears.net/new/gearknowledge/gear-design-procedure-in-practical-design/design-shapes-of-spur-gears.html>
- [8] Autodesk, “Finite element analysis (fea),” 2024. [Online]. Available: <https://www.autodesk.com/solutions/simulation/finite-element-analysis>
- [9] SolidBi, “Solidworks. qué es y para qué sirve.” [Online]. Available: <https://solid-bi.es/solidworks/>
- [10] A. Addison, “How to find denavit-hartenberg parameter tables,” 2020. [Online]. Available: <https://automaticaddison.com/how-to-find-denavit-hartenberg-parameter-tables/>
- [11] Byju, “Jacobian,” 2024. [Online]. Available: <https://byjus.com/maths/jacobian/>


- [12] W. Khalil y E. Dombre, "Modeling, identification and control of robots," pp. 1–12, 2002. [Online]. Available: <https://www.sciencedirect.com/book/9781903996669/modeling-identification-and-control-of-robots>
- [13] J. Ichnowsk, "Configuration space visualization of 2-d robotic manipulator," 2010. [Online]. Available: <https://www.cs.unc.edu/jeffi/c-space/robot.xhtml>
- [14] M. babaias, "Task space and workspace for robots," 2021. [Online]. Available: <https://mecharithm.com/learning/lesson/task-space-and-workspace-for-robots-102>
- [15] C. Voltage, "Uno r3 development board," 2024. [Online]. Available: <https://www.controlvoltage.net/arduino-uno-r3-development-board.html>
- [16] Vayuyaan, "5v single channel (one channel) relay module for arduino." [Online]. Available: <https://vayuyaan.com/shop/electronic-modules/5v-single-channel-one-channel-relay-module-for-arduino/>
- [17] Hallroad, "12v dc diaphragm vacuum air pump," 2024. [Online]. Available: <https://hallroad.pk/product/12v-dc-diaphragm-vacuum-air-pump-in-pakistan/>
- [18] P. Electronics, "Motor nema 17." [Online]. Available: <https://www.electronicsecuador.com/producto/motor-nema-17-12a-04nm/>
- [19] Robosync, "A4988 driver stepper motor driver," 2018. [Online]. Available: <https://robosynckits.in/product/a4988-driver-stepper-motor-driver-good-quality/>
- [20] ElectroPeak, "Cnc shield v3," 2022. [Online]. Available: <https://electropeak.com/arduino-cnc-shield-v3>
- [21] ModaRM, "Cámara web vmax," 2023. [Online]. Available: <https://www.modarm.com/esRW/ELECTRONICA/>
- [22] "You only look once: Unified, real-time object detection," 2016. [Online]. Available: <http://pjreddie.com/yolo/>

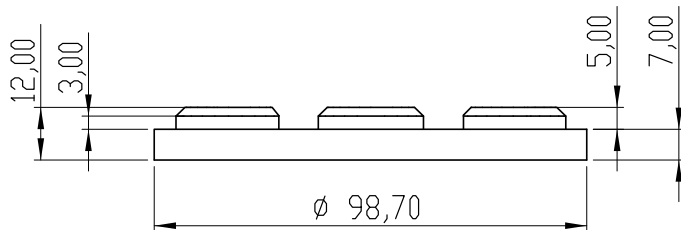
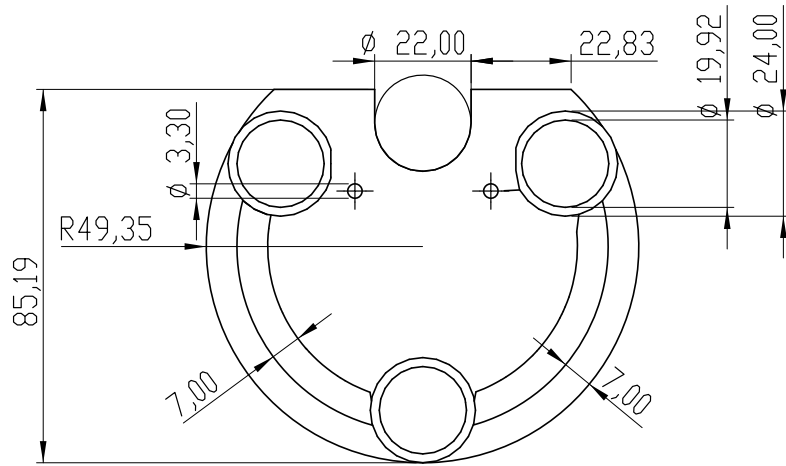
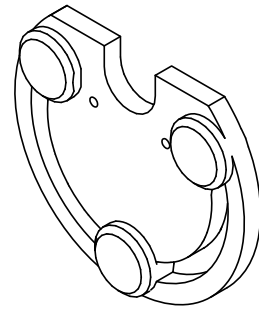
- [23] Ultralytics, "Documentación ultralytics yolov8," 2023. [Online]. Available: <https://docs.ultralytics.com/es/>
- [24] D. Amos, "Python gui programming with tkinter." [Online]. Available: <https://realpython.com/python-gui-tkinter/>
- [25] Apple, "Iphone 11 - especificaciones técnicas," 2022. [Online]. Available: <https://support.apple.com>
- [26] Roboflow, "Build and deploy computer vision models," 2023. [Online]. Available: <https://roboflow.com/>
- [27] Google, "Google colaboratory." [Online]. Available: <https://colab.google/>

Appendix A
Mechanical drawings



13	C4	BELL	1	PLA	D03-110	3D PRINTED
12	C4	LINK SUPPORT	1	PLA	D03-109	3D PRINTED
11	C4	ENDLESS SCREW	1	STAINLESS STEEL	-	-
10	C3	LINK #1	1	PLA	D03-108	3D PRINTED
9	C2	LINK#2	1	PLA	D03-107	3D PRINTED
8	C2	COUPLING OF LINK#2	1	PLA	D03-106	3D PRINTED
7	E2	BASE	1	PLA	D03-105	3D PRINTED
6	C1	MOTOR SUPPORT 2	1	PLA	D03-104	3D PRINTED
5	C1	SPACER 8MM	2	PLA	D03-103	3D PRINTED
4	C1	MOTOR SUPPORT 1	1	PLA	D03-102	3D PRINTED
3	B2	STEEL ROD	3	STAINLESS STEEL	-	STEEL ROD 8MMx400MM
2	A1	MOTOR	3	VARIOUS	-	NEMA 17 40MM MOTOR
1	A1	UPPER BASE	1	PLA	D03-101	3D PRINTED

UIDE	 MECHATRONICS ENGINEERING	DIB. CERECEREZ G.	15/01/2024
		REV. MOYA M.	15/01/2024
		REV. MOSSUERA G.	15/01/2024
CHOCOBOT 2.0		D03 - 001	
		ESCALA: 1:2,5	



SPECIFICATION FOR PRINTING

MATERIAL: PLA
 PROCESS: FDM
 PRINTER: ARTILLERY SIDEWINDER X1
 FILLING TYPE: TRIANGULAR
 FILL PERCENTAGE: 20%
 COLOUR/MARK: BLACK/SKP3D
 BED TEMPERATURE: 55 C°
 EXTRUSION TEMPERATURE: 215 C°
 LAYERS: INITIAL AND FINAL 3

TREATMENT: NO TREATMENT

COATING: UNCOATED

UIDE

MECHATRONICS ENGINEERING

MATERIAL:

PLA

TOL.GRAL:
±0,2

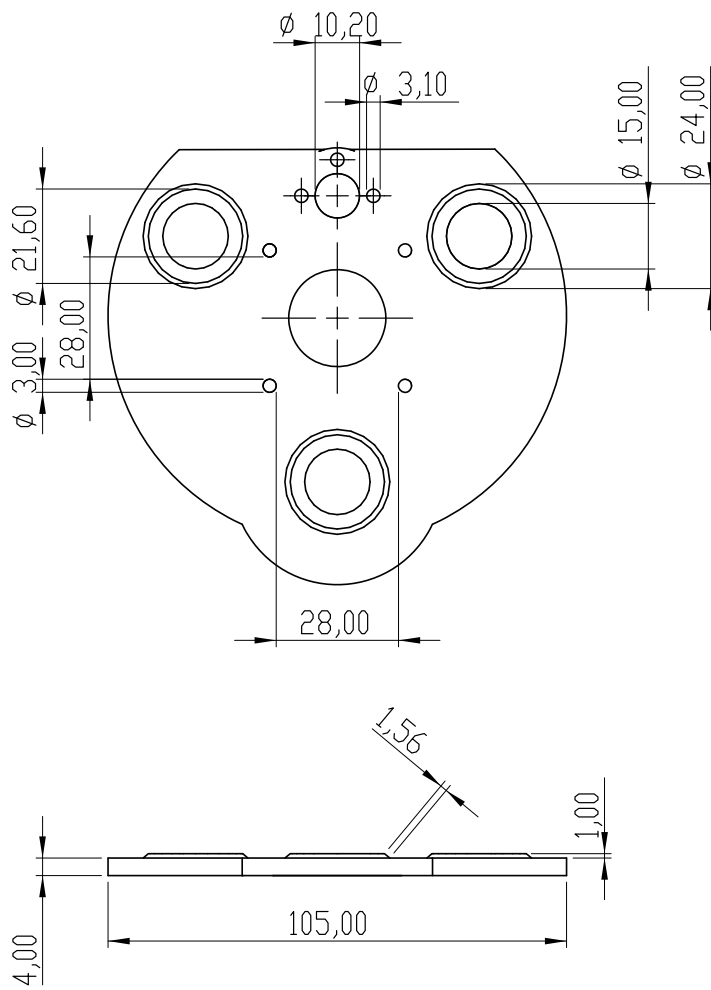
SCALE:
1:1,5

DIB	CERECEREZ G.	15/01/2024	
REV.	MDYA M.	15/01/2024	
REV.	MOSQUERA G.	15/01/2024	

UPPER BASE

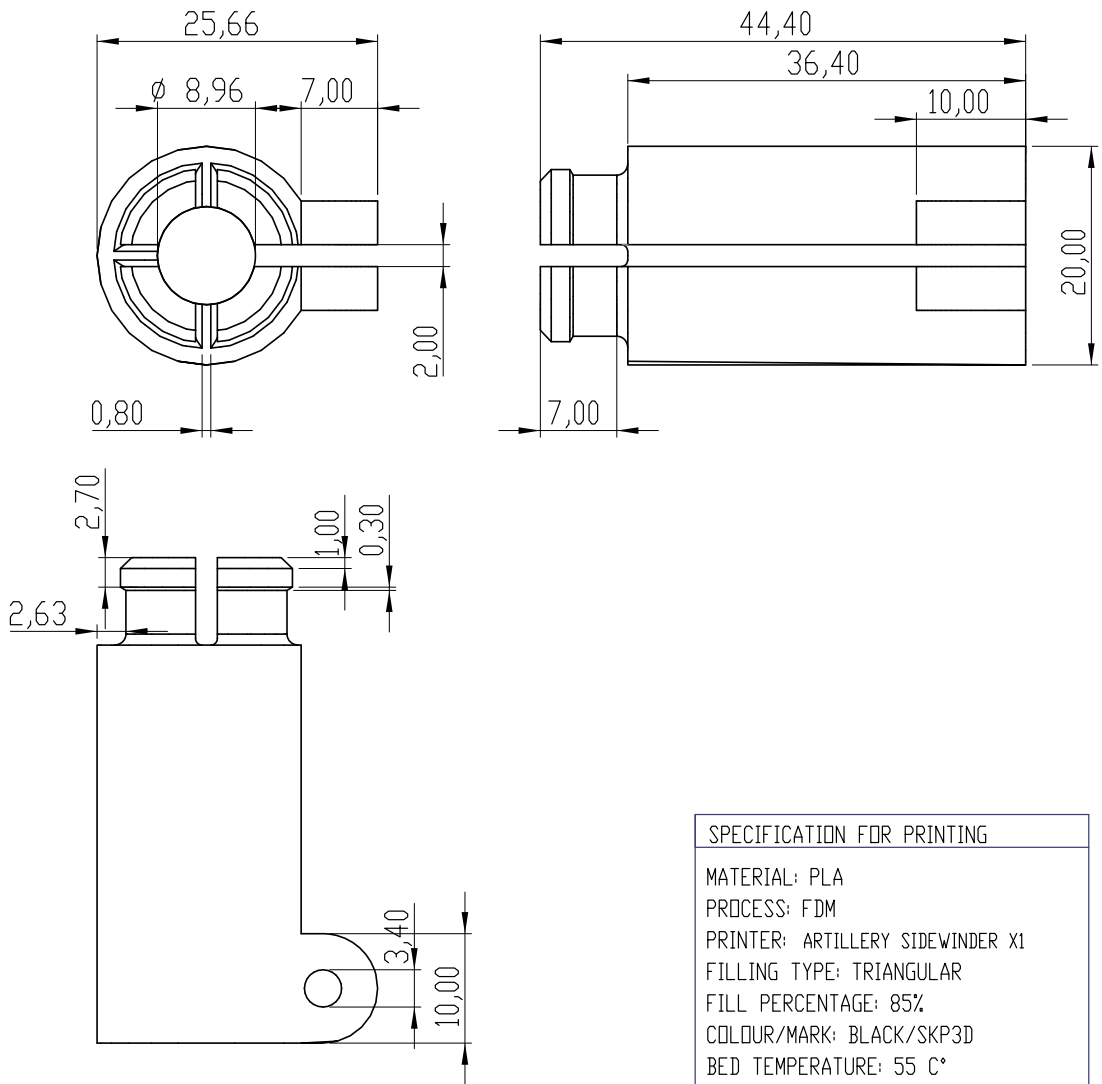
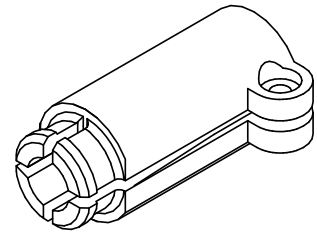
D03-101





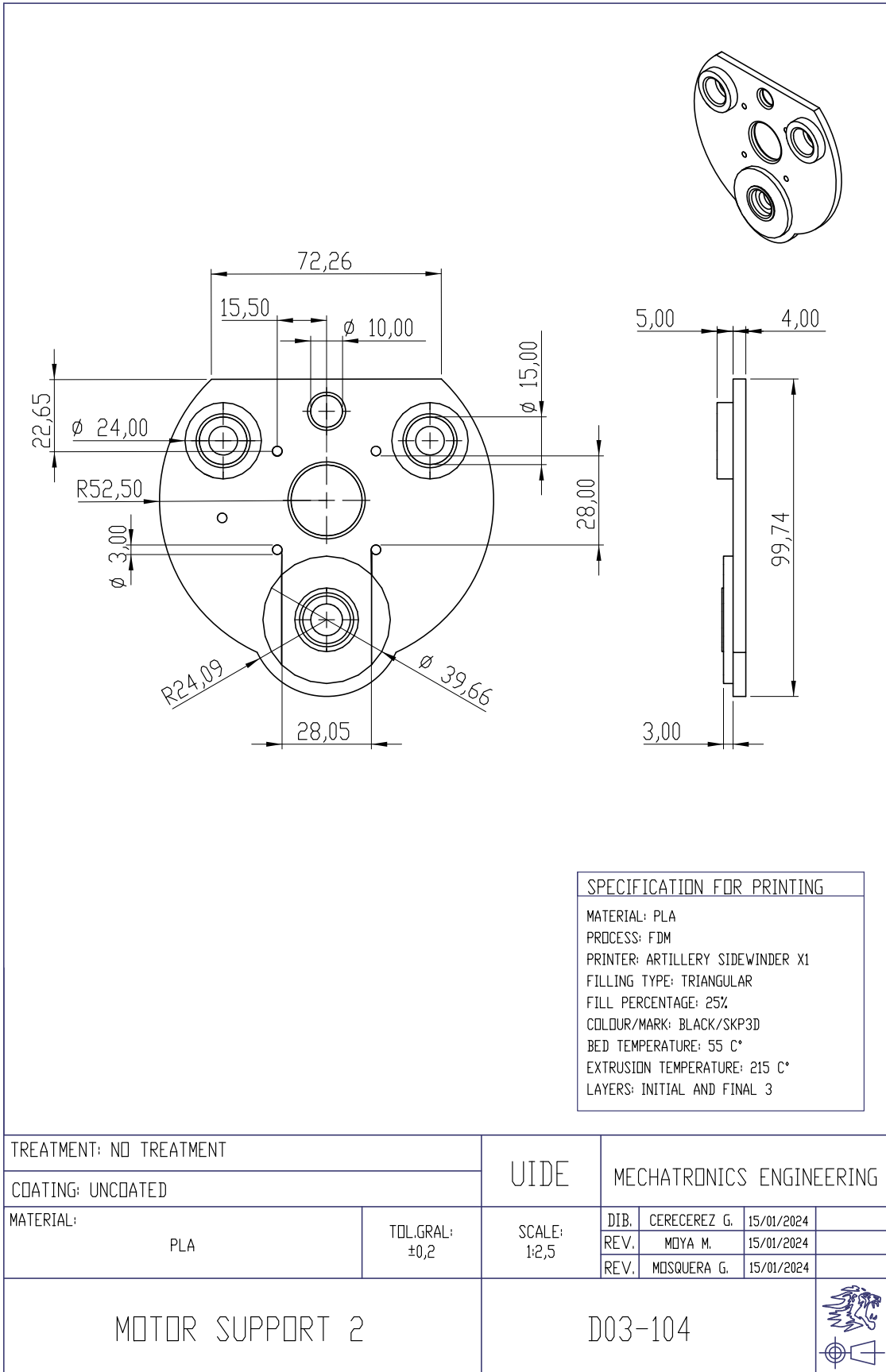
SPECIFICATION FOR PRINTING			
MATERIAL:	PLA		
PROCESS:	FDM		
PRINTER:	ARTILLERY SIDEWINDER X1		
FILLING TYPE:	TRIANGULAR		
FILL PERCENTAGE:	25%		
COLOUR/MARK:	BLACK/SKP3D		
BED TEMPERATURE:	55 C°		
EXTRUSION TEMPERATURE:	215 C°		
LAYERS:	INITIAL AND FINAL 4		

TREATMENT: NO TREATMENT		UIDE	MECHATRONICS ENGINEERING			
COATING: UNCOATED						
MATERIAL:	PLA	TOL.GRAL: ±0,2	SCALE: 1:2,5	DIB.	CERECEREZ G.	15/01/2024
				REV.	MOYA M.	15/01/2024
				REV.	MOSQUERA G.	15/01/2024
MOTOR SUPPORT 1			D03-102			



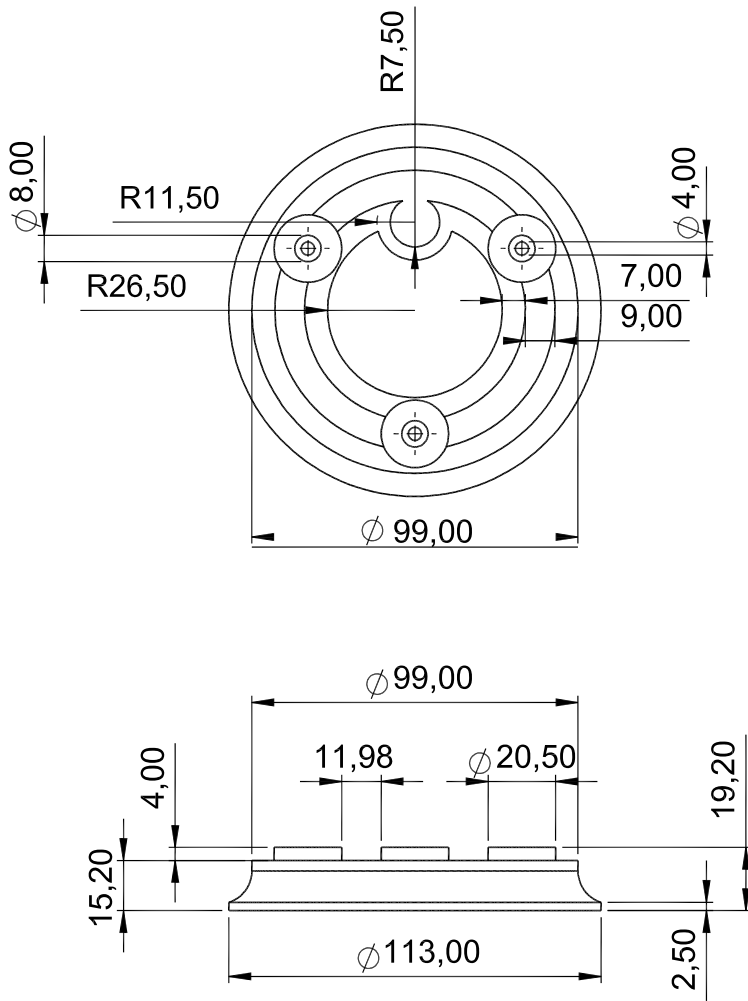
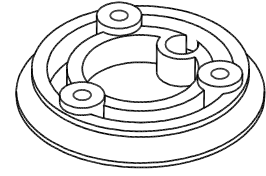
SPECIFICATION FOR PRINTING			
MATERIAL:	PLA		
PROCESS:	FDM		
PRINTER:	ARTILLERY SIDEWINDER X1		
FILLING TYPE:	TRIANGULAR		
FILL PERCENTAGE:	85%		
COLOUR/MARK:	BLACK/SKP3D		
BED TEMPERATURE:	55 C°		
EXTRUSION TEMPERATURE:	215 C°		
LAYERS:	INITIAL AND FINAL 3		

TREATMENT: NO TREATMENT		UIDE	MECHATRONICS ENGINEERING		
COATING: UNCOATED					
MATERIAL:	PLA	TOL.GRAL: ±0,2	SCALE: 2:1	DIB.	CERECEREZ G. 15/01/2024
				REV.	MOYA M. 15/01/2024
				REV.	MOSQUERA G. 15/01/2024
SPACER 8MM			D03-103		



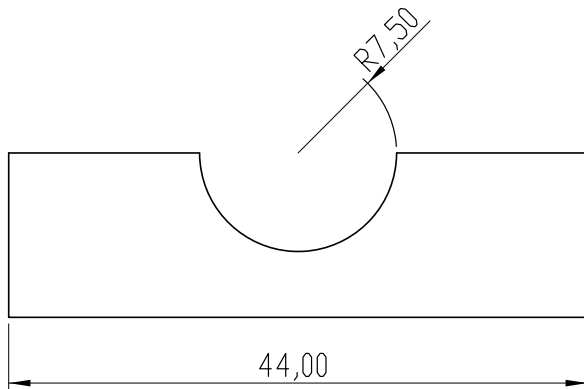
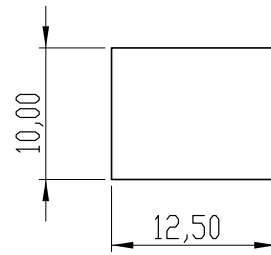
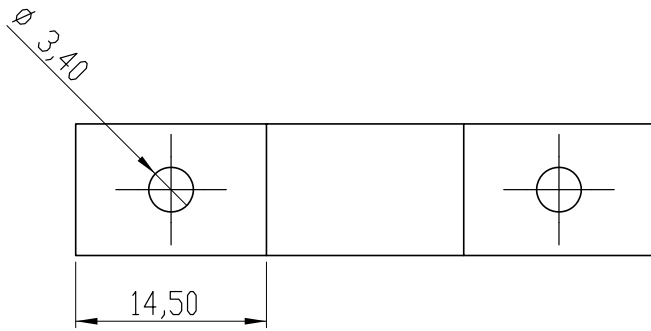
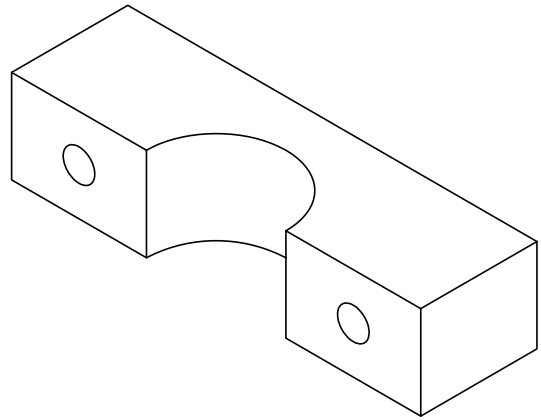
SPECIFICATION FOR PRINTING	
MATERIAL:	PLA
PROCESS:	FDM
PRINTER:	ARTILLERY SIDEWINDER X1
FILLING TYPE:	TRIANGULAR
FILL PERCENTAGE:	25%
COLOUR/MARK:	BLACK/SKP3D
BED TEMPERATURE:	55 C°
EXTRUSION TEMPERATURE:	215 C°
LAYERS:	INITIAL AND FINAL 3

TREATMENT: NO TREATMENT		UIDE	MECHATRONICS ENGINEERING						
COATING: UNCOATED									
MATERIAL:	PLA	TOL.GRAL:	±0,2	SCALE:	1:2,5	DIB.	CERECEREZ G.	15/01/2024	
						REV.	MOYA M.	15/01/2024	
						REV.	MOSQUERA G.	15/01/2024	
MOTOR SUPPORT 2				D03-104					





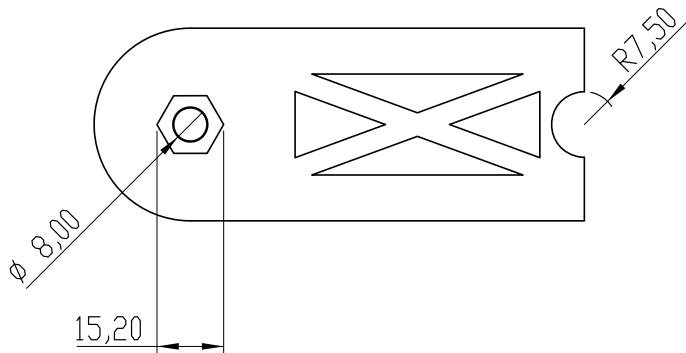
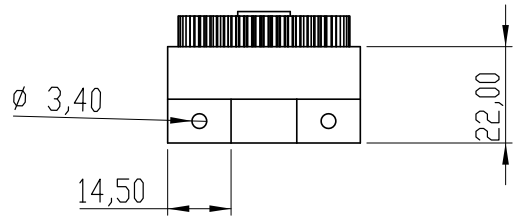
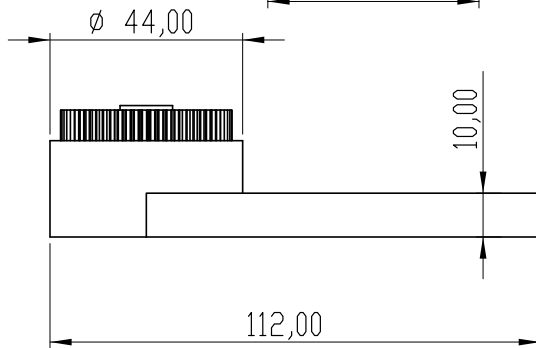
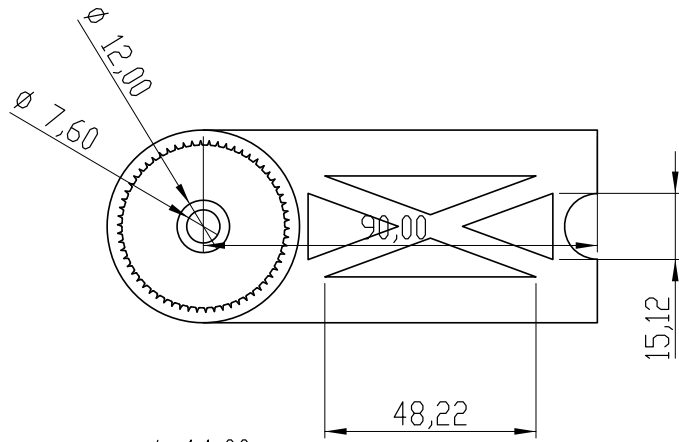
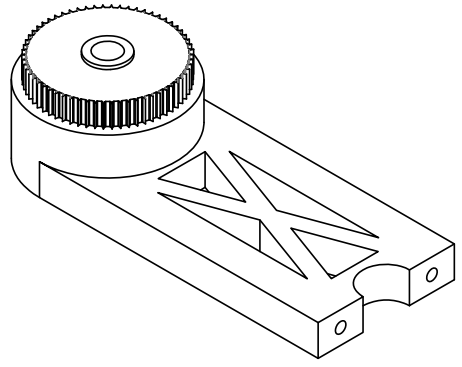
SPECIFICATION FOR PRINTING			
MATERIAL:	PLA		
PROCESS:	FDM		
PRINTER:	ARTILLERY SIDEWINDER X1		
FILLING TYPE:	TRIANGULAR		
FILL PERCENTAGE:	25%		
COLOUR/MARK:	BLACK/SKP3D		
BED TEMPERATURE:	55 C°		
EXTRUSION TEMPERATURE:	215 C°		
LAYERS:	INITIAL AND FINAL 4		

TREATMENT: NO TREATMENT		UIDE	MECHATRONICS ENGINEERING			
COATING: UNCOATED						
MATERIAL:	PLA	TOL.GRAL: $\pm 0,2$	SCALE: 1:2,5	DIB.	CERECEREZ G.	15/01/2024
				REV.	MOYA M.	15/01/2024
				REV.	MOSQUERA G.	15/01/2024
BASE			D03-105			



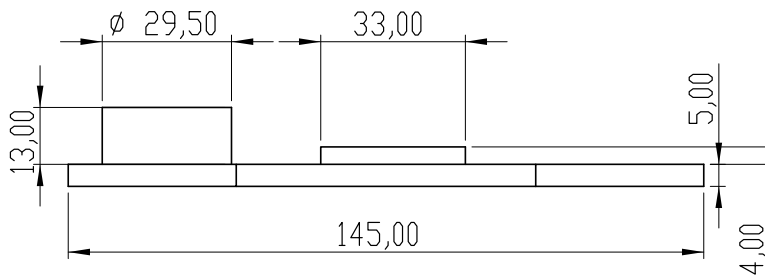
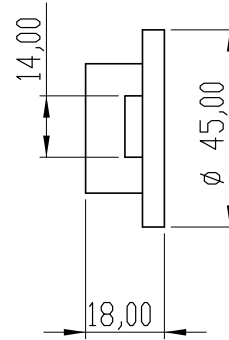
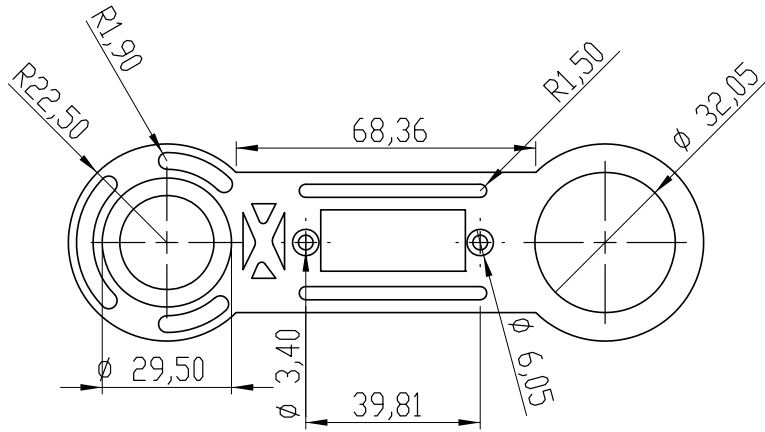
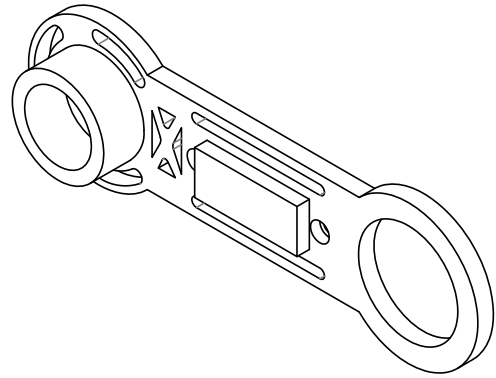
PRINTING SPECIFICATION			
MATERIAL:	PLA		
PROCESS:	FDM		
PRINTER:	ARTILLERY SIDEWINDER X1		
FILLING TYPE:	TRIANGULAR		
FILLING PERCENTAGE:	25%		
COLOR/BRAND:	BLUE/ESUN		
BED TEMPERATURE:	60 C°		
EXTRUSION TEMPERATURE:	215 C°		
LAYERS:	INITIAL 3-FINAL 3		

TREATMENT: NO TREATMENT		UIDE	MECHATRONICS ENGINEERING		
COVERING: NO COVERING					
MATERIAL: PLA	TOL.GRAL: ±0,2	SCALE: 2:1	DIB.	CERECEREZ G.	15/01/2024
			REV.	MOYA M.	15/01/2024
			REV.	MOSQUERA G.	15/01/2024
COUPLING OF LINK #2		D03-106			 



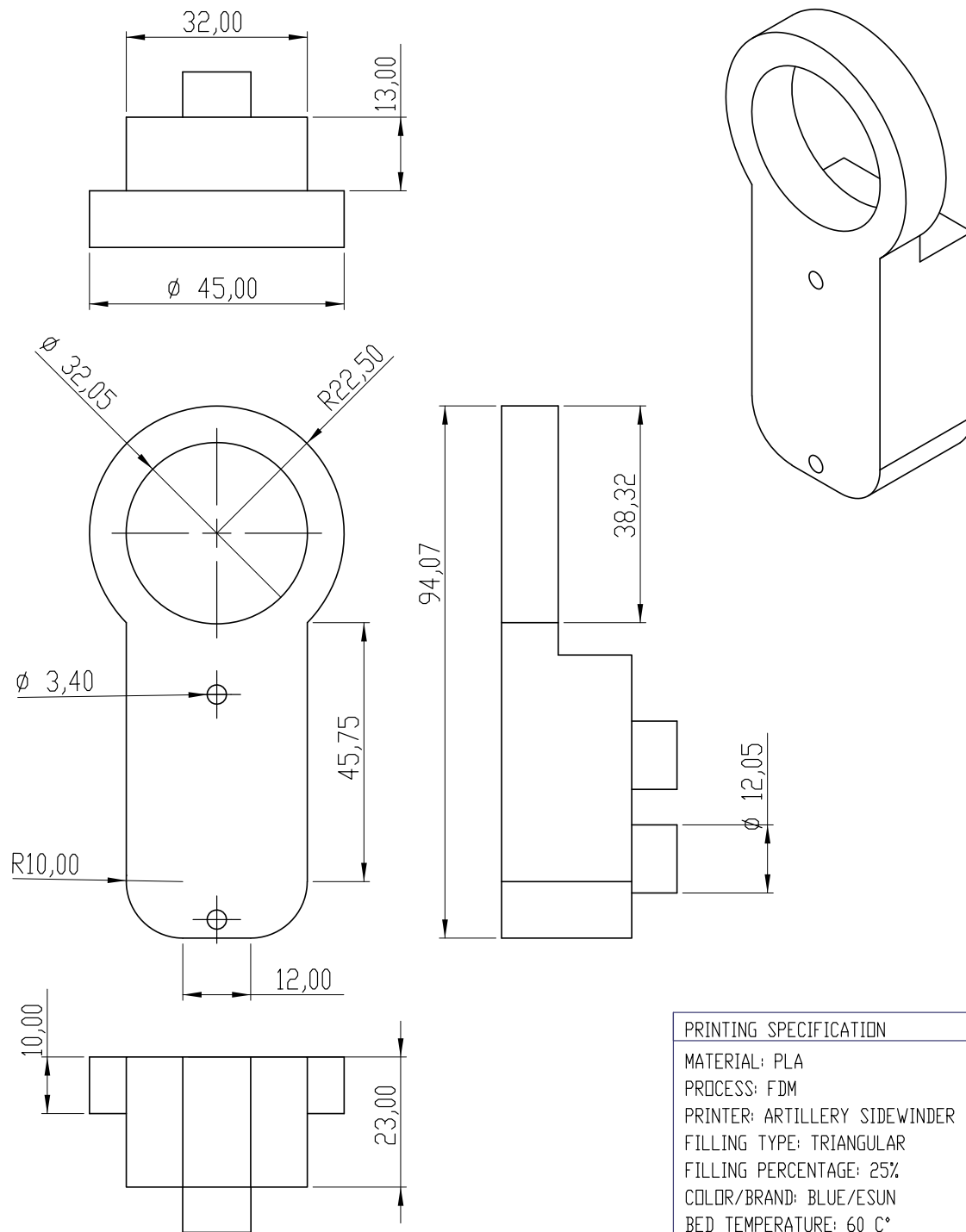
PRINTING SPECIFICATION			
MATERIAL:	PLA		
PROCESS:	FDM		
PRINTER:	ARTILLERY SIDEWINDER X1		
FILLING TYPE:	TRIANGULAR		
FILLING PERCENTAGE:	25%		
COLOR/BRAND:	BLUE/ESUN		
BED TEMPERATURE:	60 C°		
EXTRUSION TEMPERATURE:	215 C°		
LAYERS:	INITIAL 3-FINAL 3		

TREATMENT: NO TREATMENT		UIDE	MECHATRONICS ENGINEERING			
COVERING: NO COVERING						
MATERIAL:	PLA	TOL.GRAL:	SCALE:	DIB.	CERECEREZ G.	15/01/2024
		±0,2	1:1,5	REV.	MOYA M.	15/01/2024
				REV.	MOSQUERA G.	15/01/2024
LINK #2			D03-107			



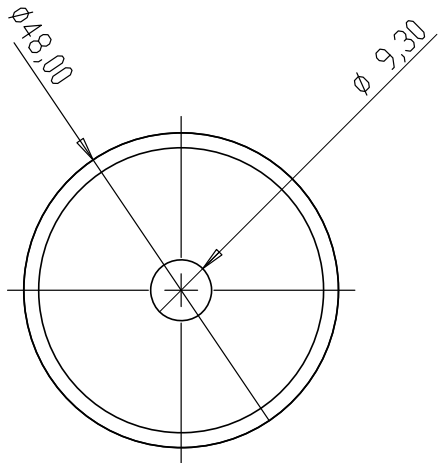
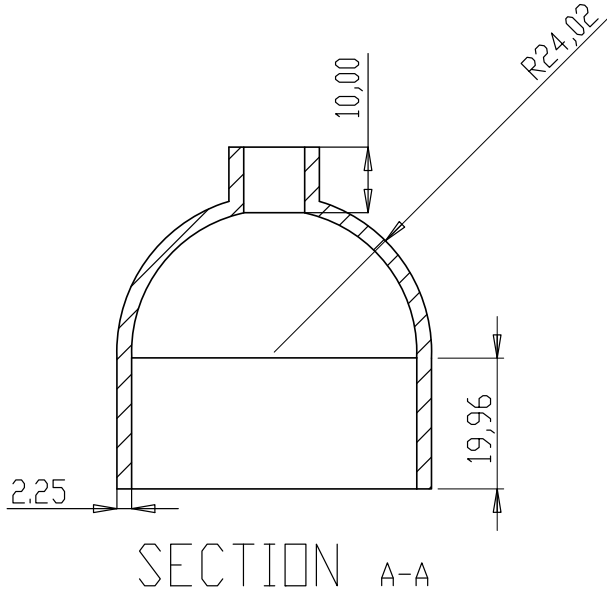
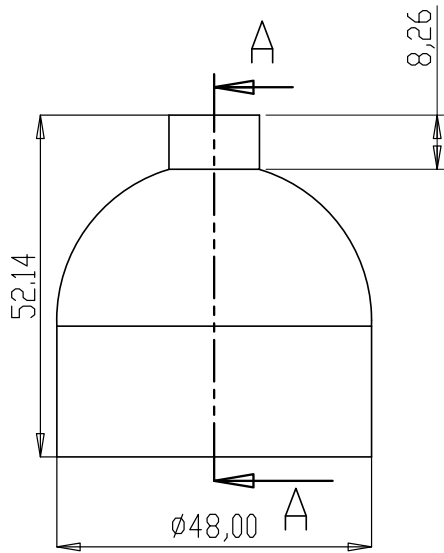
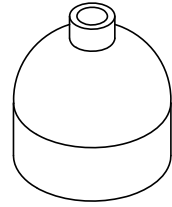
PRINTING SPECIFICATION			
MATERIAL: PLA			
PROCESS: FDM			
PRINTER: ARTILLERY SIDEWINDER X1			
FILLING TYPE: TRIANGULAR			
FILLING PERCENTAGE: 25%			
COLOR/BRAND: BLUE/ESUN			
BED TEMPERATURE: 60 C°			
EXTRUSION TEMPERATURE: 215 C°			
LAYERS: INITIAL 3-FINAL 3			

TREATMENT: NO TREATMENT		UIDE	MECHATRONICS ENGINEERING		
COVERING: NO COVERING					
MATERIAL: PLA		TOL.GRAL: ±0,2	SCALE: 1:1,5	DIB. CERECEREZ G.	15/01/2024
				REV. MDYA M.	15/01/2024
				REV. MOSQUERA G.	15/01/2024
LINK #1			D03-108		



PRINTING SPECIFICATION			
MATERIAL:	PLA		
PROCESS:	FDM		
PRINTER:	ARTILLERY SIDEWINDER X1		
FILLING TYPE:	TRIANGULAR		
FILLING PERCENTAGE:	25%		
COLOR/BRAND:	BLUE/ESUN		
BED TEMPERATURE:	60 C°		
EXTRUSION TEMPERATURE:	215 C°		
LAYERS:	INITIAL 3-FINAL 3		

TREATMENT: NO TREATMENT		UIDE	MECHATRONICS ENGINEERING			
COVERING: NO COVERING						
MATERIAL:	PLA	TOL.GRAL: ±0,2	SCALE: 1:1	DIB.	CERECEREZ G.	15/01/2024
				REV.	MOYA M.	15/01/2024
				REV.	MOSQUERA G.	15/01/2024
LINK SUPPORT			D03-109			

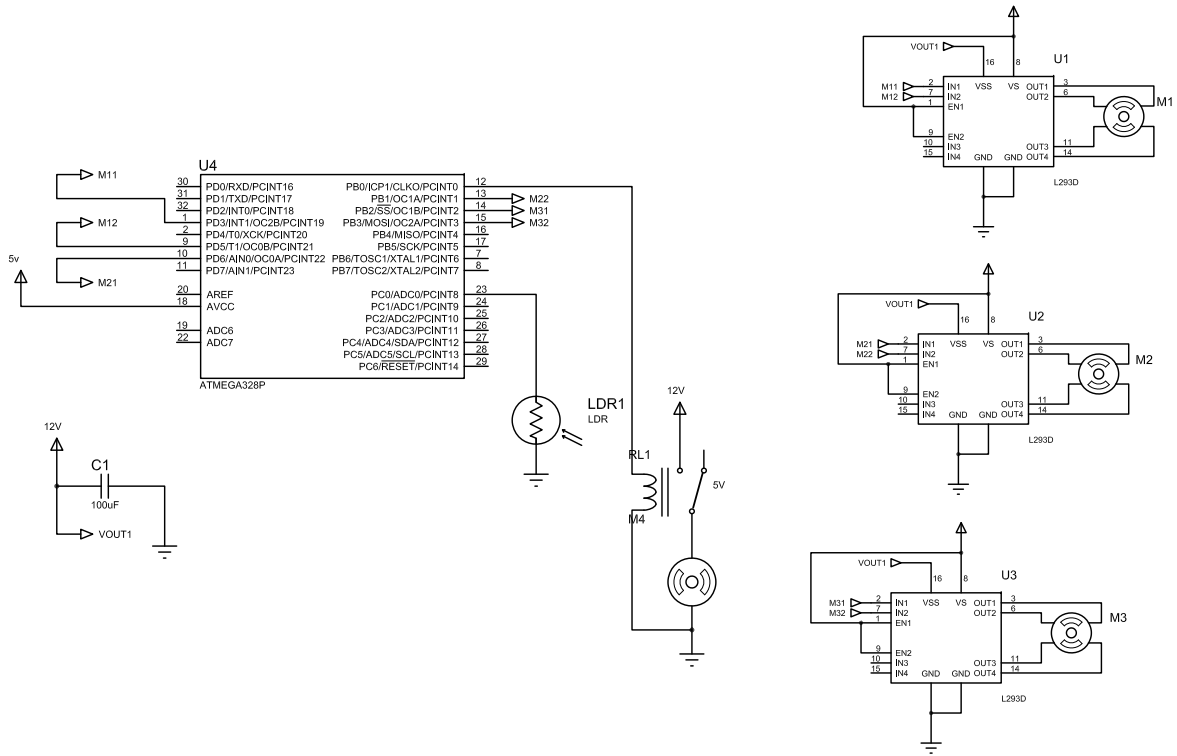



PRINTING SPECIFICATION			
MATERIAL: PLA			
PROCESS: FDM			
PRINTER: ARTILLERY SIDEWINDER X1			
FILLING TYPE: TRIANGULAR			
FILLING PERCENTAGE: 25%			
COLOR/BRAND: BLUE/ESUN			
BED TEMPERATURE: 60 C°			
EXTRUSION TEMPERATURE: 215 C°			
LAYERS: INITIAL 3 - FINAL 3			

TREATMENT: NO TREATMENT		UIDE	MECHATRONIS ENGINEERING			
COVERING: NO COVERING						
MATERIAL: PLA		TOL.GRAL: ±0,2	SCALE: 1:1	DIB.	CERECEREZ G	15/01/2024
				REV.	MOYA M.	15/01/2024
				REV.	MOSQUERA G.	15/01/2024
BELL			D03-110			



Appendix B
Electronic drawings



UIDE	 MECHATRONICS ENGINEERING	DIB. CERECEREZ G.	15/01/2024
		REV. MOYA M.	15/01/2024
		REV. MOSQUERA G.	15/01/2024
CHOCOBOT 2.0 ELECTRONIC DRAWING		D02 - 001	
		SCALE: N/A	